A TRANSIENT ANALYSIS OF STAGNATION REGION IN A FUEL DROPLET COMBUSTION

by

R. VENKATESH

DEPARTMENT OF AERONAUTICAL ENGINEERING
INDIAN INSTITUTE OF TECHNOLOGY KANPUR

APRIL, 1975

A TRANSIENT ANALYSIS OF STAGNATION REGION IN A FUEL DROPLET COMBUSTION

A Thesis Submitted
In Partial Fulfilment of the Requirements
for the Degree of
MASTER OF TECHNOLOGY

by

R. VENKATESH

to the

DEPARTMENT OF AERONAUTICAL ENGINEERING
INDIAN INSTITUTE OF TECHNOLOGY KANPUR
APRIL, 1975

AE-1975-M-VEN-TRA

CERTIFICATE

This is to certify that the work for the thesis entitled, 'A Transient Analysis of Stagnation Region in a Fuel Droplet Combustion', has been carried out by Mr. R. Venkatesh under my supervision and that it has not been submitted elsewhere for a degree.

O P Sharma

(DR. O.P. SHARMA)
Assistant Professor
Department of
Aeronautical Engineering
Indian Institute of Technology,
Kanpur.

ACKNOWLEDGEMENT

I wish to express my deep sense of gratitude to Dr. O.P. Sharma, for his constructive criticism and encouraging guidance at every phase of this work.

I am very much indebted to Mr. V.K. Nema, Ph.D. student in the Department of Aeronautical Engineering, for his help as well as the confidence, he has inspired in me, from time to time.

I also thank Mr. T.S. Jayaraman and Mr. T.S. Sreedharan, Senior Scientists at V.S.S.C., Trivandrum and all other friends who extended their help at different stages.

R. VENKATESH

ABSTRACT

The combined phenomena of forced convective motion and of transient burning of a liquid fuel droplet in an oxidizing atmosphere is studied. The analysis is restricted to the stagnation point governed by the unsteady boundary layer flow equations which are solved numerically to obtain detailed flow field for pentaborane droplets. The effect of various parameters on the unsteady burning process is determined. It is found that the non-equilibrium vaporization kinetics plays the most dominant part in determining the transient behaviour. Some discussion of the time scales of different physical processes present in this problem is also given.

CONTENTS

NOMENCLATURE

A		Pre-exponential frequency factor, Eq. (II-18)
B		Transfer number, Eq. (I-2)
B_i		Reaction rate function for ith species
C	$=$	$\rho\mu/\rho_e\mu_e$, Chapman-Rubesin function
C_p		Specific heat at constant pressure of the gaseous mixture, cal/gm-$^\circ$K
C_ℓ		Specific heat for the liquid fuel, cal/gm-$^\circ$K
$C_{p,i}$		Specific heat at constant pressure of the ith species
C_j		Concentrations of the reactant j, moles/cm^3
D		Binary diffusion coefficient in the Fick's law, cm^2/sec
D_{ij}		Binary diffusion coefficient between the species i and j, cm^2/sec
E		Activation energy for gaseous chemical reaction, cal/mole
f		Non-dimensional modified stream function, Eq. (II-42)
f_s		Non-dimensional modified stream function at the interface, Eq. (II-62)
f'		Non-dimensional velocity (= p)
G		Nonlinear function in g_i defined in Eq. (III-2)
h		Step length along η-axis
h_i		Enthalpy of the ith species, cal/gm
H_ℓ		Latent heat of vaporization, cal/gm
k		Specific reaction rate coefficient

$K = (A\, t_f / \rho_e^{-1} W_O W_F)$

K_o Burning rate coefficient, Eq. (I-3)

$\dot{m}$ Mass burning rate of fuel droplet, gm/sec

M Number of maximum mesh points in η-direction

n_o Order of reaction

N Number of species taking part in the chemical reaction
Also number of maximum mesh points in τ-direction

p Pressure of the gaseous mixture, gmf/cm^2. Also, $p = f'$

Pr Prandtl number $(= \frac{\mu C_p}{\lambda})$

q Heat conducted normal to the droplet surface, cal/sec

q_r Heat of combustion at the reference conditions, cal

q^o Standard heat of reaction at temperature T^o, cal/gm

$Q_{vap} = H_\ell / C_p T_e$

$Q = q_r / (\nu_F W_F C_p T_e)$

r Distance from droplet surface, cm (Fig. 2). Also $(\Delta\tau / h^2)$ in Chapter III

R^o Universal gas constant, cal/g-mole ^oK

Re Reynolds number

Sc Schmidt number $(= \mu/(\rho D))$

t Time, secs

t_f Characteristic flow time, secs, $[dU_e/dx]^{-1}$

T Temperature of the gaseous mixture, ^oK

T_ℓ Liquid temperature, ^oK

u x-component of velocity, cm/sec

U_e Free stream velocity, cm/sec

v y-component of velocity, cm/sec

V_i y-component of diffusion velocity for the ith species, cm/sec

$\dot{w}_i$ Mass rate of formation of ith species per unit volume, gm/cm^3-sec

W_i Molecular weight of ith species, gm/mole

$\overline{W}$ Average molecular weight of the gaseous mixture, gm/mole

x Coordinate along the droplet surface, (Fig. 4)

y Coordinate perpendicular to the droplet surface, (Fig. 4)

Y_i Mass fraction of ith species in the gaseous mixture

α_o Power of oxidizer mass fraction in the reaction rate expression

β_F Power of fuel mass fraction in the reaction rate expression

$\Delta\tau$ Dimensionless time increments

ϵ Non-dimensional evaporation coefficient

$\varepsilon = E/RT_e$

$\varepsilon_v = H_\ell/R^oT_{\ell,o}$

η Transformed y-coordinate perpendicular to the droplet surface, Eq. (II-40)

η_ℓ Transformed y-coordinate perpendicular to the droplet surface in the liquid phase, Eq. (II-52)

$\Delta\eta$ Non-dimensional grid spacing in η-direction

θ Non-dimensional temperature in gas phase, $(= T/T_e)$

θ_ℓ Non-dimensional temperature in liquid phase, $(= T_\ell/T_e)$

λ Coefficient of thermal conductivity of the gaseous mixture in the boundary layer, cal/cm-sec ^{o}K

λ_ℓ Coefficient of thermal conductivity of liquid fuel, cal/cm-sec ^{o}K

μ Coefficient of viscosity of the gaseous mixture, gm/cm-sec

ν_i' Stochiometric coefficient for the ith reactant

ν_i'' Stoichiometric coefficient for the ith product species

ξ Transformed x-coordinate along the droplet surface

ρ Density of gaseous mixture in the boundary layer, gm/cm^3

ρ_ℓ Density of liquid fuel, gm/cm^3

τ Ratio of actual time to the characteristic flow time, $(= t/t_f)$

$\varphi = [(\rho_e \lambda_e C_p)/(\rho_\ell \lambda_\ell C_\ell)]$, Eq. (II-61)

ψ Stream function

Subscripts:

e Free stream conditions

eq Equilibrium value

F Fuel

i Mesh point along η-axis (in Chapter III). Also, species i (= O, F, P)

ℓ Liquid phase

n Mesh point along τ-axis (in Chapter III)

O Oxidizer

s Interface, (y or η = 0)

st.pt. Stagnation point

o(zero) Initial reference conditions

Superscripts:

k	Iteration index (number of iteration cycle)
–	Average values
'	First differential with respect to η
"	Second differential with respect to η
o	Reference or initial conditions

LIST OF FIGURES

CHAPTER I

INTRODUCTION

I.A. GENERAL BACKGROUND

The study of the combustion of liquid fuels plays a very important role in the design of several engineering systems like industrial furnaces, diesel engines, jet engines, liquid propellant rocket motors, etc. In fact the liquid fuels form a considerable portion of the total energy requirements of the world. Therefore an understanding of the combustion phenomena becomes essential for efficient as well as pollution-free working of these devices.

As an illustration of the motivation to investigate the combustion process of liquid fuels, the phenomena of combustion instability is described next very briefly. Liquid-propellant rocket engines of various types are generally designed to deliver a fairly constant steady thrust for a duration that may extend from several seconds to as much as few hours. However, in many cases the result is not the desired steady operation and instead combustion often becomes rough under different circumstances. This is mainly due to large pressure oscillations in the combustion chamber. Frequencies ranging from 10 cycles/sec to as much as 5000 cycles/sec

have been observed in the oscillographs. In most of the cases these sustained oscillations were not truely periodic in nature over a wide frequency range, but seemed to be merely a series of random fluctuations. Not only is the thrust vibration, which results from the aperiodic oscillation in the combustion chamber, undesirable from the standpoint of possible damage to the structural elements or instruments in the vehicle but in extreme cases failure of the powerplant itself can occur.

In the above-mentioned situations the unsteady operation is attributed to the so called combustion instability, which is a complex phenomenon involving the interaction of the combustion process with flow oscillations within the combustor. Combustion instability initiated by a flow disturbance results in a perturbation of steady state combustion process. Consequently the rate of energy released by the combustion process may increase and a part of it is fed back into the initial flow disturbance, resulting in a form of coupling between chamber pressure and energy addition to the chamber under a proper phase. The feed back loop so established between the combustion process and the flow oscillations results in a self-sustained oscillation of the gases within the combustor. In the majority of the cases the occurrence of combustion instability results in the destruction of the engine or failure of the mission supported by the engine. Therefore it becomes essential to investigate the detailed mechanism of combustion energy release and its

coupling to the accoustic phenomena in order to suppress this instability.

In most of the propulsion devices, the liquid fuel is introduced into the combustion chamber in the form of liquid droplets of varying sizes. The treatment of the combustion of liquid sprays is a very complicated problem involving several poorly known variables like distribution of the sizes of the droplets, density of droplets in the spray, etc. It has been found convenient both theoretically and experimentally to investigate in details the burning of an isolated droplet, and then to apply these results for obtaining the burning characteristics of liquid sprays.

Earliest investigations dealing with the liquid droplets concerned with the vaporization rates only (1). However during the past two decades the problem of liquid droplet combustion has been analyzed extensively under different sets of simplifying assumptions (see, for example, references 2-14). A brief description of the physical phenomena and the assumptions frequently made in determining the steady-state burning rate of a liquid droplet in a stagnant atmosphere will help to clarify the nature of the problem (8).

A typical theoretical analysis is based on the following assumptions: (i) Spherical symmetry; (ii) No body forces; (iii) Fick's law of binary diffusion, (iv) Negligible radiant heat transfer; and (v) The transport parameters

depending upon various transport coefficients as well as the specific heat of the mixture are considered to be independent of both temperature and composition. Suitable constant values are often used for these parameters.

A schematic model of the burning droplet is shown in Fig. 1. The physical processes resulting in the droplet combustion can be briefly stated as follows. The gaseous vapours move away from the droplet surface, mix with the gases of the surrounding environment via diffusion and convection, and then result in a zone of intense chemical activity (flame) at some distance from the liquid surface. A steady state is established in which a continuous supply of fuel (or oxidizer) vapours from the liquid surface, and the oxidant (or fuel) from the outer boundary sustain the exothermic chemical activity in the flame zone. Heat is transferred from the flame zone to the droplet surface to supply latent heat of vaporization of the liquid fuel ensuring a continuous supply of fuel vapours. A schematic representation of the detailed temperature and species mass fraction profiles is given in Fig. 2.

Early experimental work carried out by a number of workers (see, for example, references 3 and 4) had indicated that the relation between the radius of the droplet and time was well represented throughout the steady state combustion of the droplet by the so called 'd^2 law'. According to this

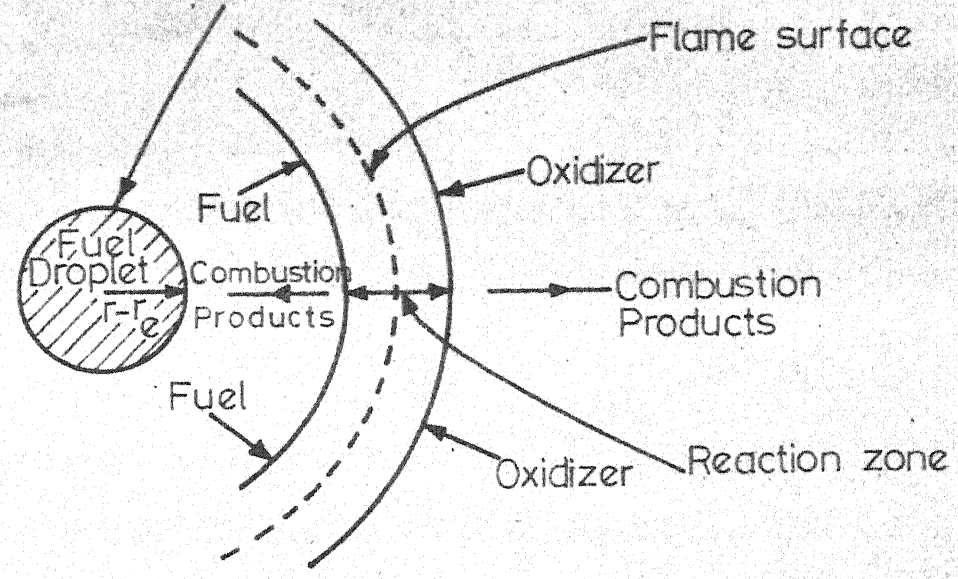

FIG. 1 – A SCHEMATIC REPRESENTATION OF STEADY STATE DROPLET BURNING IN STAGNANT OXIDIZING ATMOSPHERE

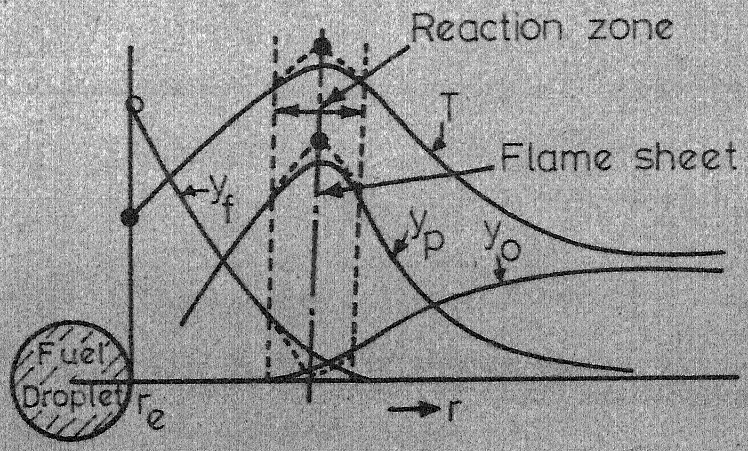

FIG. 2 – TEMPARATURE (T) AND SPECIES MASS FRACTION (OXIDIZER (y_o), FUEL (y_f) AND PRODUCTS (y_p)) PROFILES vs DISTANCE FROM DROPLET SURFACE ($r-r_e$). BROKEN STRAIGHT LINES CORRESPOND TO FLAME SHEET APPROXIMATION

law, the time rate of change of the square of the droplet diameter remains constant (known as the evaporation constant) which means that the mass burning rate is directly proportional to the droplet radius. Under the assumption of infinitely fast reaction rate (also known as flame sheet approximation), the flame zone reduces to an infinitesimal thickness and is represented by a surface. As a consequence of this approximation, some explicit expressions have been obtained for the burning rate of fuel droplets and the temperature at the flame front under the assumption of constant as well as variable transport properties (5, 6, and 14). A typical and widely quoted solution based on temperature independent transport properties is given below (8),

$$\dot{m} = 4\pi r_\ell \, \bar{\rho}\bar{D} \, \ell n \, (1 + B) \qquad \ldots (I\text{-}1)$$

where B is the so called transfer number given by

$$B = \frac{1}{H_\ell} \{\bar{C}_p (T_\infty - T_\ell) + \frac{q^\circ Y_{O\infty}}{W_O \nu_O}\} \qquad \ldots (I\text{-}2)$$

The other symbols are defined under the heading Nomenclature. These theoretical results agree very well with the experimental observations on steady-state burning.

However, almost in all practical spray combustion systems, the burning takes place under the forced convective conditions, and in addition, the combustion phenomena, for an appreciable fraction of the total droplet lifetime, remains

transient. It has been found that the pollutant formation in auto-engines, and the combustion instability phenomena are generally affected significantly by the transient processes. In the present analysis an unsteady model was used to treat the burning of liquid fuel droplets in an oxidizing atmosphere under forced convection. Before going into the details of the present analysis, it may be useful to review some of the important past contributions dealing with these two aspects of the droplet combustion.

I.B. REVIEW OF THE RELATED PAST CONTRIBUTIONS

Although a number of theoretical analyses have been done on the combustion of isolated single liquid fuel droplets in an oxidizing atmosphere during the past two decades, there are still very few attempts dealing with the combined phenomena of transient burning and of forced convective motion. A brief description of the past work investigating these effects separately is given below.

At the very early stages, it was realized that the spherical symmetry of the droplets could not be achieved because of the presence of natural or forced convection effects. An early attempt to determine the influence of forced convection experimentally was made by Gohrbandt (9). The mass evaporation rate of camphor spheres was found proportional to the radius and the square root of Reynolds number. Spalding (3)

applied the concept of boundary layer to take into account the contributions of both natural and forced convection. He established an empirical relation to predict mass burning rate under the influence of forced convection by performing experiments on spheres over a range of Reynolds number varying from 800 to 4000. Several other empirical relations incorporating forced convection have been found out since then (14). For example, more recently Faeth and Lazar (12) obtained the following correlation in terms of the burning coefficients,

$$K_{(\text{forced convection})} = K_0\left[1 + 0.278 Re^{1/2} Pr^{1/3}\left(1 + \frac{1.237}{Re\ Pr^{4/3}}\right)^{-\frac{1}{2}}\right], \quad \ldots (I\text{-}3)$$

which was found consistent with the experimental data in the range $10 < Re < 800$, and also the theoretical prediction of Fendall et.al (10). Recently Bruzustowski and Natarajan (11) studied experimentally the evaporation and combustion of cold n-pentane droplets injected into a hot oxidizing gas at moderate pressures with high speed motion picture photography and were able to correlate their results in terms of transfer number, Reynolds number and Nusselt number.

Simultaneously there have been some attempts to study separately the transient aspects of the problem. Several of them deal with the supercritical conditions of the liquid phase such that the droplet is treated simply as a puff of gaseous material diffusing into the surrounding

environment (14-19). The burning of droplets under such conditions is highly transient in nature and moreover the usual theories to determine the combustion phenomena becomes highly inaccurate. Spalding (15) first considered this case by treating the liquid droplet as a point source of gas injected instantaneously into an infinite medium and predicted the burning rates which are valid at high pressures. Rosner (16) modified Spalding's results by considering finite size gas sources. Later Chervinsky (17) extended the analysis by including the convective terms and the variable density. He obtained solutions of the flow field around a burning droplet in the Von-Mises plane using flame sheet approximation. Recently Polymeropoulos and Perkin (18) extended this model further by including the finite rate chemistry. Rosner and Chang (19) investigated the transient evaporation and combustion of a fuel droplet near its critical temperature and showed the inadequacies in the past analyses based on the familiar quasi-steady approximation.

There are a few investigations dealing with other transient phenomena associated with liquid phase evaporation or combustion in stagnant environment under normal (non-critical) conditions (14,15,20-23). Kirkaldy (20) first tried to solve the time dependent heat and mass transfer equations by assuming slow evaporation so that the convective term in the equations disappear. His analysis was restricted to the

phenomena of condensation without any chemical activity. Spalding (15) also obtained analytical expressions for the combustion of a fuel droplet at high pressures by assuming uniform properties including constant density. Strahle (21) employed perturbation method to the unsteady spherical symmetric burning problem by representing the dependent variables as power series in which the leading terms were time independent. However, the first order time dependent solution was obtained assuming a constant density throughout the flow field. Chervinsky (22) obtained the detailed solutions for the fuel mass concentration and temperature fields in the Von-Mises plane as well as the burning rate as a function of time by employing flame sheet approximation. Kotake and Okazaki (23) obtained numerical solutions for unsteady vaporization and combustion of a fuel droplet in quiescent air assuming infinite kinetic rate reaction. It is shown that the process of evaporation and combustion are influenced greatly by the initial conditions of the air surrounding the droplet and that the combustion process approaches a quasi-steady state near its end while the process of evaporation cannot attain a quasi-steady state of mass and heat transfer at the droplet surface.

To investigate the combined phenomena of transient burning and of forced convective motion of the oxidizing gas relative to the droplet, Strahle (24) employed the unsteady

boundary layer flow approximation to the forward stagnation point of a vaporizing droplet and then obtained approximate solutions by using an integral approach. Like Kotake and Okazaki, it was found that the development of thermal layer within the liquid did not attain a steady state during the typical droplet lifetimes. For accurate analyses, the transient vaporization kinetics must be included.

In the present analysis a fully unsteady model is used to deal with the combined phenomena of forced convective motion and of transient burning of a liquid droplet. The treatment is however restricted to the stagnation point in view of the resulting computational simplification as well as the fact that it can also represent qualitatively the essential features of the entire droplet combustion process. However, the procedure is easily extendable to other regions of the flow field around the droplet. The unsteady conservation equations of species concentration, velocity, and temperature of gaseous mixture surrounding the droplet and of temperature within the droplet are solved by finite difference scheme which is more exact compared to that of an integral approach. Accurate detailed profiles for velocity, temperature, and species concentration are obtained as a result of this analysis. The various time scales which play an important role during the transient combustion of a liquid fuel droplet are described. The details of the present analysis is given in the next chapter.

CHAPTER II

FORMULATION OF THE PROBLEM

II.A. PHYSICAL MODEL

In general, the liquid fuels or propellants are injected through orifices into the combustion chamber in the form of liquid jets. These jets soon breakup into tiny droplets. Upon ignition of the spray, droplets vaporize resulting in a supply of gaseous fuel and oxidizer. These vapours mix with each other and react forming hot combustion products. Consider a single fuel droplet in the spray which undergoes transient burning in a forced convective oxidizing environment of the combustion chamber. Due to the flow of hot oxidizing gases at temperature T_e and pressure P_e with a velocity U_e relative to the droplet, a boundary layer is developed over the surface of the liquid fuel droplet (see Fig. 3). However, in the wake region, the boundary layer approximation breaks down and the analysis of the flow field becomes highly complicated. The boundary layer flow portion is treated as laminar for the purpose of this analysis. In reality the turbulent conditions are more likely to prevail. However, this can be taken into account phenomenologically in the numerical analysis developed for the present model by the introduction of proper exchange coefficients for viscosity,

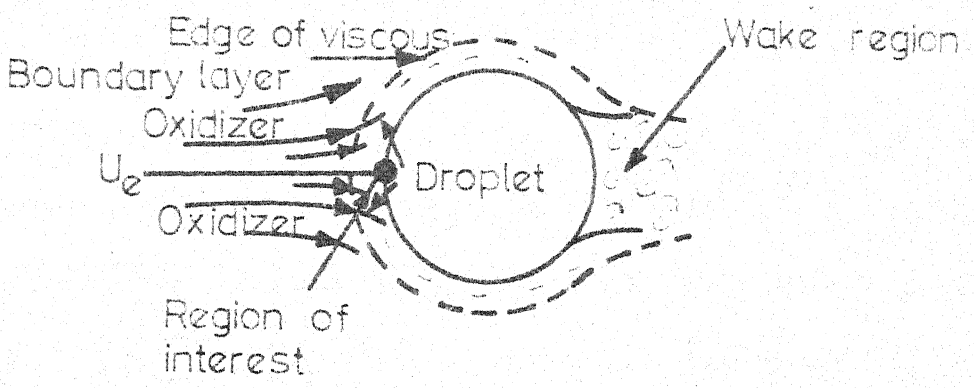

FIG. 3 – SCHEMATIC REPRESENTATION OF THE FLOW FIELD AROUND A SPHERICAL DROPLET.

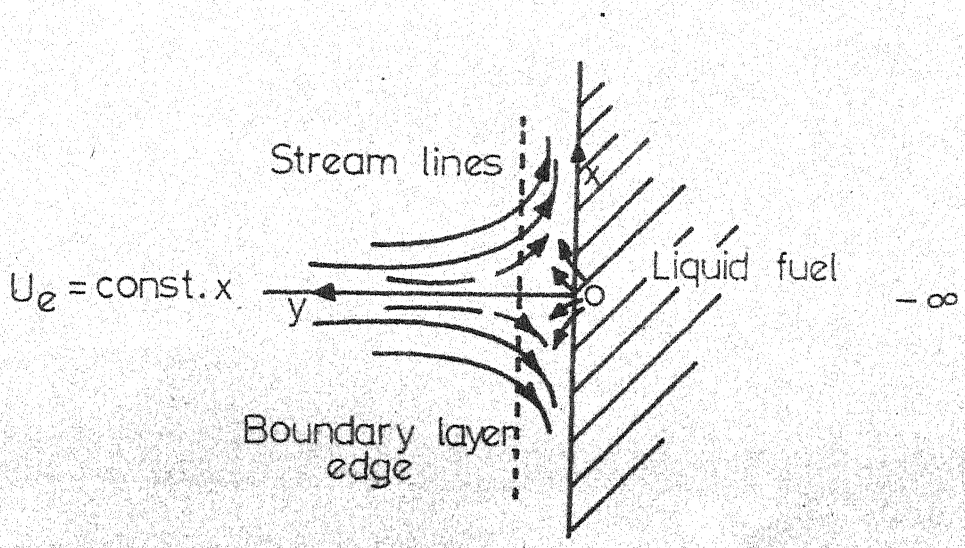

FIG. 4 – SCHEMATIC REPRESENTATION OF TWO DIMENSIONAL STAGNATION POINT FLOW FIELD ON A VAPOURIZING SURFACE AS APPROXIMATED IN THE PRESENT MODEL.

thermal conductivity, and coefficient of diffusion in the governing equations.

Initially, after ignition, the fuel evaporates from the liquid surface, diffuses outwards and mixes with the gaseous oxidizer diffusing inwards from the surrounding free stream. With the passage of time heat is liberated as a result of exothermic reaction taking place between the gaseous oxidizer and the fuel vapour inside the boundary layer. The heat so liberated further augments the process of vaporization. Therefore the transient burning of a liquid fuel droplet in a forced convective environment involves the solution of unsteady boundary layer flow equations coupled with the heat and mass transfer conditions at the surface. For simplicity, the present analysis is restricted to stagnation point of the liquid fuel droplet.

As far as the droplet interior is concerned, it is assumed that no circulation of fluid occurs and that there is no mixing of the liquid fuel with the oxidizer or product species. In other words, only heat conducted within the fuel droplet is included in the analysis. Moreover, it is also assumed that at the centre of the droplet the temperature does not change which implies that the thermal diffusion layer at the liquid fuel droplet surface is much thinner compared to its radius. Also, when the analysis is restricted to the stagnation point, the temperature gradient along the

droplet surface is neglected compared to the gradient in the perpendicular direction.

The flow configuration representing schematically unsteady burning process analysed in the present model is shown in Fig. 4. The origin is fixed at the stagnation point O. x and y axes represent the distances along and perpendicular to the droplet surface respectively. Dotted line shown in Fig. 4 indicates the edge of the boundary layer. It is clear that the stagnation point flow approximation reduces the spatial dependence of the partial differential equations by unity. Due to symmetry, all the dependent variables can be chosen to be functions of y alone, except U_e which must be taken proportional to x.

The detailed mathematical formulation is described in the next section.

II.B. MATHEMATICAL FORMULATION

II.B.1 Governing Equations:

The governing equations for the chemically reacting two-dimensional, unsteady boundary-layer flow can be expressed as follows (see, for example, reference 8):

Continuity:

$$\frac{D\rho}{Dt} + \rho \vec{\nabla} \cdot \vec{u} = 0 \qquad \text{II-1}$$

Momentum Conservation:

$$\rho \frac{Du}{Dt} = -\frac{dp}{dx} + \frac{\partial}{\partial y}\left(\mu \frac{\partial u}{\partial y}\right)$$

Energy Conservation:

$$\rho \frac{Dh}{Dt} = u \frac{dp}{dx} - \frac{\partial q}{\partial y} + \mu\left(\frac{\partial u}{\partial y}\right)^2$$

Species Conservation:

$$\rho \frac{DY_i}{Dt} = -\frac{\partial}{\partial y}\left(\rho Y_i V_i\right) + \dot{w}_i \qquad i = 1,2,\ldots$$

Equation of state for a mixture of ideal gases:

$$p = \sum_{i=1}^{N} \left(\frac{\rho_i}{W_i}\right) R^o T$$

And the total derivative,

$$\frac{D(\ )}{Dt} = \left[\frac{\partial(\ )}{\partial t} + u \frac{\partial(\ )}{\partial x} + v \frac{\partial(\ )}{\partial y}\right]$$

The symbols used in the above equations are defined under the heading Nomenclature.

The continuity equation is simplified by neglecting the local variation of the mixture density with respect to time as compared to its spatial gradients. Then Eq. (II-1) reduces to

$$\frac{\partial}{\partial x}(\rho u) + \frac{\partial}{\partial y}(\rho v) = 0$$

Since the pressure gradient in a boundary layer is impressed by the external stream, we have

$$\rho_e U_e \left(\frac{dU_e}{dx}\right) = -\frac{dp}{dx} \qquad \text{(II-8)}$$

Substituting Eq. (II-8) in Eq. (II-2), the momentum conservation equation becomes

$$\rho \frac{Du}{Dt} = \rho_e U_e \left(\frac{dU_e}{dx}\right) + \frac{\partial}{\partial y}\left(\mu \frac{\partial u}{\partial y}\right) \qquad \text{(II-9)}$$

In general expressions for the y-components of the heat flux vector (q), and of the diffusion velocity of species i (V_i) are known from the molecular theory of gases in terms of the other dependent variables. Here we will consider highly simplified form of these expressions as discussed below.

Consider the general expression for diffusion velocity for a multicomponent gaseous mixture due to concentration gradients only (8)

$$\sum_{j=1}^{N} \frac{Y_j}{W_j D_{ij}} (\vec{V}_i - \vec{V}_j) = \sum_{j=1}^{N} \frac{Y_j}{W_j} \left(\frac{\vec{\nabla} Y_j}{Y_j} - \frac{\vec{\nabla} Y_i}{Y_i}\right), \qquad i \neq j, \quad i = 1,2,\ldots,N \qquad \text{(II-10)}$$

If we assume all D_{ij} and W_{ij} to be equal, then the above equation reduces to

$$Y_i \vec{V}_i = -D_i \vec{\nabla} Y_i \qquad \text{(II-11)}$$

which is the well known Fick's law for binary diffusion. Therefore the y-component of diffusion velocity in Eq. (II-4) is expressed as

$$V_i = -\frac{D}{Y_i}\left(\frac{\partial Y_i}{\partial y}\right) \qquad \text{(II-12)}$$

Next, the heat flux vector for a multicomponent mixture comprises of two mechanisms, namely, the heat conduction and the thermal energy carried by interdiffusing species. This can be expressed as

$$\vec{q} = -\lambda \vec{\nabla} T + \rho \sum_{i=1}^{N} h_i Y_i \vec{V}_i \qquad \text{(II-13)}$$

Here we have neglected the contribution due to thermal diffusion of species. Therefore, the y-component of the heat flux vector, q, in Eq. (II-3) is approximated by

$$q = -\lambda \frac{\partial T}{\partial y} + \rho \sum_{i=1}^{N} h_i Y_i V_i \qquad \text{(II-14)}$$

where V_i is given in Eq. (II-12).

It is convenient to express the energy conservation equation, Eq. (II-3), in terms of temperature (T), and for this purpose, it is further assumed that the specific heats at constant pressure of different species are nearly the same and can be replaced by an average value independent of temperature, that is, $C_{p,i} = C_p$ = constant; for all i. Then making use of Eqs. (II-12) and (II-14), we can rewrite Eq. (II-3) as follows

$$\rho C_p \frac{\partial T}{\partial t} + \rho C_p \left(u \frac{\partial T}{\partial x} + v \frac{\partial T}{\partial y}\right) = \mu \left(\frac{\partial u}{\partial y}\right)^2 + u \frac{dp}{dx} + \frac{\partial}{\partial y}\left(\lambda \frac{\partial T}{\partial y}\right) - \sum_{i=1}^{N} h_i^o \dot{w}_i \qquad \text{(II-15)}$$

In order to express the source terms involving $\dot{w}_i$ in Eqs. (II-4) and (II-15), we approximate the chemical reactions taking place in the flame zone by an overall single step reaction of the following type:

$$\nu_O[O] + \nu_F[F] \rightarrow \nu_{P,1}[P_1] + \nu_{P,2}[P_2] + \ldots \qquad \text{(II-16)}$$

The order of the reaction for a given combination of fuel and oxidizer is determined from the kinetic information quoted in the literature. Now, according to the law of mass action, the net rate of production per unit volume of the i^{th} chemical species, $\dot{w}_i$, is given by

$$\dot{w}_i = W_i(\nu_i'' - \nu_i')\dot{w} = W_i(\nu_i'' - \nu_i')k \prod_{j=1}^{N} (C_j)^{\nu_j'},$$

$$i = [O], [F], [P_1], \ldots, \qquad \text{(II-17)}$$

where the specific reaction rate coefficient k is approximated by the Arrhenius expression,

$$k = Ae^{-E/R^oT} \qquad \text{(II-18)}$$

we will let a suitable effective value $n_o = \sum_{j=1}^{N} \nu_j' = (\alpha_o + \beta_F)$ to represent the order of the reaction in the following analysis.

Having obtained a detailed expression for $\dot{w}_i$, we can now express the term $\sum_{i=1}^{N} h_i^o \dot{w}_i$ in terms of other variables as follows:

$$\sum_{i=1}^{N} h_i^o \dot{w}_i = \dot{w} \sum_{i=1}^{N} W_i(\nu_i'' - \nu_i')h_i^o = \dot{w}\, q_r \qquad \text{(II-19)}$$

Here q_r stands for the heat of combustion at the reference conditions. In view of Eqs. (II-12), (II-17), (II-18), and (II-19), the species conservation equations, Eq. (II-4) and the energy conservation equation, Eq. (II-15), become

$$\rho \frac{\partial Y_O}{\partial t} + \rho u \frac{\partial Y_O}{\partial x} + \rho v \frac{\partial Y_O}{\partial y} = \frac{\partial}{\partial y}(\rho D \frac{\partial Y_O}{\partial y}) - (\frac{\nu_O A}{W_O^{\alpha_O - 1} W_F^{\beta_F}}) \rho^{n_O} Y_O^{\alpha_O} Y_F^{\beta_F} e^{-E/R^O T} \quad \text{(II-20)}$$

$$\rho \frac{\partial Y_F}{\partial t} + \rho u \frac{\partial Y_F}{\partial x} + \rho v \frac{\partial Y_F}{\partial y} = \frac{\partial}{\partial y}(\rho D \frac{\partial Y_F}{\partial y}) - (\frac{\nu_F A}{W_O^{\alpha_O} W_F^{\beta_F - 1}}) \rho^{n_O} Y_O^{\alpha_O} Y_F^{\beta_F} e^{-E/R^O T} \quad \text{(II-21)}$$

$$\rho C_p \frac{\partial T}{\partial t} + \rho C_p (u \frac{\partial T}{\partial x} + v \frac{\partial T}{\partial y}) = u \frac{dp}{dx} + \mu (\frac{\partial u}{\partial y})^2 + \frac{\partial}{\partial y}(\lambda \frac{\partial T}{\partial y}) - \dot{w} q_r \quad \text{(II-22)}$$

It is convenient and consistent with the simplifications introduced above to assume a constant average molecular weight ($\overline{W}$) for the mixture. Then, the equation of state for ideal mixture, Eq. (II-5), becomes

$$p = \rho R^O T / \overline{W} \quad \text{(II-23)}$$

Next equation governing the heat transfer within the liquid fuel droplet is discussed. Neglecting the temperature gradient in the x-direction compared to that in the y-direction, the unsteady heat conduction equation for the

liquid droplet can be expressed as

$$\rho_\ell C_\ell \frac{\partial T_\ell}{\partial t} = \frac{\partial}{\partial y}\left(\lambda_\ell \frac{\partial T_\ell}{\partial y}\right) \qquad \text{(II-24)}$$

Note that the droplet surface is regressing inwards at a rate equal to the vaporization rate. For the non-equilibrium vaporization rate, the mass lost by evaporation per unit time per unit surface area can be expressed as (8)

$$\rho_s v_s = \epsilon p \sqrt{\frac{\bar{W}}{2\pi R^o T_s}} \left[(Y_{F,s})_{eq} - Y_{F,s}\right] \qquad \text{(II-25)}$$

here $(Y_{F,s})_{eq}$ denotes the equilibrium mass fraction of the fuel vapour at the surface corresponding to the temperature T_s and pressure p. ϵ , the evaporation coefficient is defined as the ratio of the observed rate of evaporation to the evaporation rate calculated from the Knudsen equation. When the liquid is in equilibrium with the vapour, the equilibrium vapour pressure of the fuel $(p_{F,eq})$ can be related to the temperature of the liquid (T_ℓ) with the help of Clapeyron equation as follows (8)

$$\left(\frac{p_{F,eq}}{p^o_{F,eq}}\right) = \exp\left[\frac{H_\ell}{R^o T_{\ell,o}}\left(1 - \frac{T_{\ell,o}}{T_s}\right)\right] \qquad \text{(II-26)}$$

where $p^o_{F,eq}$ denotes the value of $p_{F,eq}$ at the initial temperature $(T_{\ell,o})$ of the liquid. Note that the above relation is applicable when both phases contain only one species. Furthermore, it is assumed that H_ℓ is constant. In otherwords, any temperature dependence of the heat of transition per mole (H_ℓ) has been

neglected. Thus $(Y_{F,s})_{eq}$ in Eq. (II-25) can be expressed with the help of Eq. (II-26) as follows:

$$(Y_{F,s})_{eq} = (Y_{F,s})^{o}_{eq} \exp\left[\frac{H_\ell}{R^{o}T_{\ell,o}}\left(1 - \frac{T_{\ell,o}}{T_s}\right)\right] \qquad \text{(II-27)}$$

where $(Y_{F,s})^{o}_{eq}$ denotes the equilibrium mass fraction of fuel vapours at the surface corresponding to the initial temperature of the droplet T^{o}_{ℓ}.

In order to fix gas-liquid interface at y = 0 the liquid surface is continuously translated towards the interface at a velocity equal to the instantaneous regression rate due to vaporization ($v_{\ell,s}$). Due to incompressible nature of the liquid any interface pressure fluctuations caused by this motion are considered negligible. Introducing a modified y-coordinate, the unsteady heat conduction equation within the droplet, Eq. (II-24), then becomes

$$\rho_\ell C_\ell \left[\frac{\partial T_\ell}{\partial t} + v_{\ell,s}\frac{\partial T_\ell}{\partial y_\ell}\right] = \frac{\partial}{\partial y_\ell}\left(\lambda_\ell \frac{\partial T_\ell}{\partial y_\ell}\right), \qquad t > 0, \quad 0 < y_\ell < -\infty \qquad \text{(II-28)}$$

where $y_\ell = y + \int_0^t v_{\ell,s}\, dt$. [Note that y (or y_ℓ) is negative towards the liquid phase side.] At the surface, from mass conservation, we have the relationship

$$\rho_\ell v_{\ell,s} = \rho_s v_s \qquad \text{(II-29)}$$

II.B.2 Boundary Conditions:

The boundary conditions for continuity and momentum equations are easily expressible in terms of the velocity components as follows:

At the droplet surface, y = 0:

$$u = 0 \qquad \text{(No slip condition)} \qquad \text{(II-30)}$$

$$v = v_s(x,t) \qquad \text{(Due to vaporization)} \qquad \text{(II-31)}$$

And, for away from the liquid droplet surface, $y \to \infty$:

$$u = u(x,t) \qquad \text{(II-32)}$$

The boundary conditions for the chemical species at the gas liquid interface (y = 0) are determined by mass balance at the interface. In general, the component i is being transported towards the gas-liquid interface by diffusion at the rate $(\rho D_i \frac{\partial Y_i}{\partial y})_s$, and, simultaneously it is being converted away from the interface by a normal current at the rate $(\rho v)_s (Y_{i,s})$ and toward the interface at the rate $(\rho v)_s (Y_{i,s})$ - provided, in the last case, the component i exists in the liquid phase. Thus, the boundary conditions for the oxygen and fuel mass fractions are respectively given by

$$(\rho D \frac{\partial Y_O}{\partial y})_s = (\rho v)_s (Y_{O,s}) \qquad \text{(II-33)}$$

$$(\rho D \frac{\partial Y_F}{\partial y})_s = (\rho v)_s (Y_{F,s} - 1) \qquad \text{(II-34)}$$

where we have assumed in Eq. (II-34) that the liquid droplet contains only pure fuel. Outside the boundary layer ($y \longrightarrow \infty$), it is clear that the species mass fractions must satisfy the following conditions:

$$Y_F = 0 \quad , \quad \text{and} \quad Y_O = Y_{O,e} \tag{II-35}$$

The boundary condition at the gas-liquid interface for temperature is determined by considering energy balance at the interface. The heat conducted from gases to liquid surface is equal to the sum of the heat conducted from liquid surface to the interior of the liquid and the heat absorbed for vaporization at the surface

$$\left|\left(-\lambda \frac{\partial T}{\partial y}\right)_s\right| = \left|\left(-\lambda_\ell \frac{\partial T_\ell}{\partial y}\right)_s\right| + (\rho v)_s H_\ell \tag{II-36}$$

Again, as $y \longrightarrow \infty$, we have

$$T = T_e \tag{II-37}$$

The liquid fuel droplet near the stagnation point is assumed to be like a semi-infinite mass without any internal circulation (see Fig. 4). Therefore, the temperature of the liquid far away from the surface ($y_\ell \longrightarrow -\infty$) remain at its initial constant value, that is,

$$T_\ell(-\infty, t) = T_{\ell,o} \tag{II-38}$$

This approximation is quite reasonable as long as the thermal wave penetration thickness is much smaller than the droplet radius.

The fuel droplet is instantaneously introduced into the oxidizing environment. This represents a discontinuity in the physical variables like velocity, species mass fractions and temperature which requires special care in specifying the initial conditions in order to start the numerical integration, and is described later on.

II.C TRANSFORMATION OF GOVERNING EQUATIONS

It is convenient to solve the boundary layer equations in terms of the well known independent variables introduced by Howrath and Dorodnitzyr as well as Levy and Lees in the following form (See, for example, reference, 25)

$$\xi(x) = \int_0^x \rho_e \mu_e U_e \, dx \tag{II-39}$$

$$\eta(x,y) = \frac{U_e}{\sqrt{2\xi}} \int_0^y \rho \, dy \tag{II-40}$$

In addition by introducing a stream function ψ defined by the relations

$$\rho u = \frac{\partial \psi}{\partial y}, \quad \text{and} \quad \rho v = -\frac{\partial \psi}{\partial x} \tag{II-41}$$

the continuity equation, Eq. (II-7), is identically satisfied. However, it is common to use another modified non-dimensional form of the stream function, namely,

$$f(\xi,\eta,t) = \frac{\psi}{\sqrt{2\xi}} \tag{II-42}$$

Then, from Eqs. (II-39) to (II-41), it can be easily shown that

$$\left(\frac{u}{U_e}\right) = \frac{\partial f}{\partial \eta} \tag{II-43}$$

and $$\rho v = -\left[\frac{\rho_e \mu_e U_e}{\sqrt{2\xi}} f + \sqrt{2\xi}\ \left\{(\rho_e \mu_e U_e)\left(\frac{\partial f}{\partial \xi}\right) + \left(\frac{\partial \eta}{\partial x}\right)\left(\frac{\partial f}{\partial \eta}\right)\right\}\right] \tag{II-44}$$

The time variable (t) is also non-dimensionalized by dividing it with a characteristic flow time (t_f),

$$\tau = t/t_f \tag{II-45}$$

The choice for t_f is given below in Eq. (II-54). Now transforming Eq. (II-9) and Eqs. (II-20) to (II-22) with the help of Eqs. (II-39), (II-40), and Eqs. (II-42) to (II-45), the conservation equation for momentum, fuel and oxidizer mass fractions, and temperature, respectively, become

$$\frac{\partial}{\partial \eta}\left(C \frac{\partial^2 f}{\partial \eta^2}\right) + f \frac{\partial^2 f}{\partial \eta^2} - \frac{\partial}{\partial \tau}\left(\frac{\partial f}{\partial \eta}\right) + \frac{2\xi}{U_e}\frac{dU_e}{d\xi}\left[\frac{\rho_e}{\rho} - \left(\frac{\partial f}{\partial \eta}\right)^2\right] =$$

$$2\xi\left[\frac{\partial f}{\partial \eta}\frac{\partial}{\partial \xi}\left(\frac{\partial f}{\partial \eta}\right) - \frac{\partial f}{\partial \xi}\frac{\partial^2 f}{\partial \eta^2}\right] \tag{II-46}$$

$$\frac{\partial}{\partial \eta}\left(\frac{C}{Sc}\frac{\partial Y_F}{\partial \eta}\right) + f\frac{\partial Y_F}{\partial \eta} - \frac{\partial Y_F}{\partial \tau} = B_F + 2\xi\left[\left(\frac{\partial f}{\partial \eta}\right)\frac{\partial Y_F}{\partial \xi} - \frac{\partial f}{\partial \xi}\cdot\frac{\partial Y_F}{\partial \eta}\right] \tag{II-47}$$

$$\frac{\partial}{\partial \eta}\left(\frac{C}{Sc}\frac{\partial Y_O}{\partial \eta}\right) + f\frac{\partial Y_O}{\partial \eta} - \frac{\partial Y_O}{\partial \tau} = B_O + 2\xi\left[\frac{\partial f}{\partial \eta}\cdot\frac{\partial Y_O}{\partial \xi} - \frac{\partial f}{\partial \xi}\cdot\frac{\partial Y_O}{\partial \eta}\right] \tag{II-48}$$

$$\frac{\partial}{\partial \eta}\left(\frac{C}{Pr}\frac{\partial \theta}{\partial \eta}\right) + f\frac{\partial \theta}{\partial \eta} + \frac{C\,U_e^2}{C_p T_e}\left(\frac{\partial^2 f}{\partial \eta^2}\right)^2 - \frac{\partial \theta}{\partial \tau} = -QB_F + 2\xi\left\{\frac{\partial f}{\partial \eta}\cdot\frac{\partial \theta}{\partial \xi} - \frac{\partial f}{\partial \xi}\cdot\frac{\partial \theta}{\partial \eta}\right\} \tag{II-49}$$

Here $C = (\frac{\rho\mu}{\rho_e\mu_e})$, $Pr = (\frac{\mu C_p}{\lambda})$, and $Sc = (\mu/\rho D)$ are, respectively, known as the Chapman-Rubesin function, the Prandtl number, and the Schmidt number. $Q = [q_r/(\nu_F W_F C_p T_e)]$ represents the non-dimensional heat of combustion. The source (or sink) terms B_F and B_O are given by

$$B_F = \nu_F\left[\frac{A\, t_f\, \rho_e^{n_o-1}}{W_O^{\alpha_o}\, W_F^{\beta_F-1}}\right] \theta^{1-n_o}\, Y_O^{\alpha_o}\, Y_F^{\beta_F}\, e^{-\varepsilon/\theta} \qquad \text{(II-50)}$$

$$B_O = \nu_O\left[\frac{A\, t_f\, \rho_e^{n_o-1}}{W_O^{\alpha_o-1}\, W_F^{\beta_F}}\right] \theta^{1-n_o}\, Y_O^{\alpha_o}\, Y_F^{\beta_F}\, e^{-\varepsilon/\theta} \qquad \text{(II-51)}$$

For the heat transfer equation within the fuel droplet, Eq. (II-28), we introduce another dimensionless variable in the y-direction,

$$\eta_\ell = \sqrt{\frac{\rho_\ell C_\ell}{t_f\, \lambda_\ell}}\, y_\ell \qquad \text{(II-52)}$$

So that Eq. (II-28) becomes

$$\frac{\partial^2\theta_\ell}{\partial\eta_\ell^2} - v_{\ell,s}\sqrt{\frac{\rho_\ell C_\ell t_f}{\lambda_\ell}}\left(\frac{\partial\theta_\ell}{\partial\eta_\ell}\right) - \frac{\partial\theta_\ell}{\partial\tau} = 0 \qquad \text{(II-53)}$$

where we have assumed a constant λ_ℓ.

In the region of the stagnation point, the governing equations can be highly simplified by dropping ξ-dependence altogether. Moreover, the velocity field for the external flow can then be expressed as

$$U_e = (x/t_f), \text{ and } t_f = (dU_e/dx)^{-1}_{st.pt} = \text{constant} \qquad \text{(II-54)}$$

Now the governing Eqs. (II-46) to (II-49) reduce, respectively, to the following forms:

$$(Cp')' + fp' + (\theta - p^2) - \frac{\partial p}{\partial \tau} = 0 \qquad \text{(II-55)}$$

$$\left(\frac{C}{Sc} Y_F'\right)' + fY_F' - \frac{\partial Y_F}{\partial \tau} = B_F \qquad \text{(II-56)}$$

$$\left(\frac{C}{Sc} Y_O'\right)' + fY_O' - \frac{\partial Y_O}{\partial \tau} = B_O \qquad \text{(II-57)}$$

$$\left(\frac{C}{Pr} \theta'\right) + f\theta' - \frac{\partial \theta}{\partial \tau} = - QB_F \qquad \text{(II-58)}$$

Here $(\ )'$ denotes differentiation with respect to η. Furthermore, the expression for the mass flux of the fuel vapours from the droplet surface Eq. (II-44), reduces to

$$\rho_s v_s = - \sqrt{\frac{\rho_e \mu_e}{t_f}} f_s = - \sqrt{\frac{\rho_e \lambda_e}{C_p t_f}} f_s \qquad \text{(II-59)}$$

where, for the last equality sign, Prandtl number is taken as unity. Now, making use of Eqs. (II-31) and (II-59), Eq. (II-53) becomes

$$\frac{\partial^2 \theta_\ell}{\partial \eta_\ell^2} + \frac{f_s C_\ell}{C_p \varphi^{\frac{1}{2}}} \frac{\partial \theta_\ell}{\partial \eta} - \frac{\partial \theta_\ell}{\partial \tau} = 0 , \quad \tau > 0, \quad 0 < y_\ell < - \infty \qquad \text{(II-60)}$$

where $\eta_\ell = \sqrt{\frac{\rho_\ell C_\ell}{t_f \lambda_\ell}} y_\ell$, and $\varphi = \frac{\rho_e \lambda_e C_p}{\rho_\ell \lambda_\ell C_\ell}$. $\qquad$ (II-61)

Note that y_ℓ is negative in the above equation. Similarly making use of Eqs. (II-31) and (II-59), Eq. (II-25) can be expressed as

$$f_s = \epsilon \sqrt{\frac{p t_f}{2\pi \mu_e}} \left(\frac{Y_{F,s} - (Y_{F,s})_{eq}}{\theta_s^{\frac{1}{2}}} \right) \qquad \text{(II-62)}$$

Rewriting Eq. (II-27) in terms of non-dimensional symbols, we obtain

$$(Y_{F,s})_{eq} = (Y_{F,s})^{o}_{eq} \exp[\varepsilon_v (1 - \theta_{\ell,o}/\theta_s)] \qquad \text{(II-63)}$$

Having transformed the governing equations, the boundary conditions should also be expressed in terms of the new variables. Following the same procedure, Eq. (II-30) to Eq. (II-37) then become.

At the droplet surface, $\eta = 0$:

$$f'(0) = 0 \qquad \text{(II-64)}$$

$$v = v_s = -\frac{1}{\rho_s} \sqrt{\frac{\rho_e \lambda_e}{C_p t_f}} f_s \qquad \text{(II-65)}$$

$$Y_O' = -f_s Y_{O,s} \qquad \text{(II-66)}$$

$$Y_F' = \sqrt{C}\, f_s (1 - Y_{F,s}) \qquad \text{(II-67)}$$

$$\theta' = \sqrt{\varphi}\, \theta_\ell' - Q_{vap} f_s \qquad \text{(II-68)}$$

And at the edge of the boundary layer, $\eta \longrightarrow \infty$:

$$f' = 1 \qquad \text{(II-69)}$$

$$Y_O = Y_{O,e} \qquad \text{(II-70)}$$

$$Y_F = 0 \qquad \text{(II-71)}$$

$$\theta = 1 \qquad \text{(II-72)}$$

Also, the boundary condition in the liquid phase, Eq. (II-38), can be rewritten as

$$\text{At } \eta_\ell \longrightarrow -\infty : \qquad \theta_\ell = \theta_{\ell,o} \tag{II-73}$$

For the initial conditions, the solutions obtained in reference (24) for an impulsively produced boundary layer flow have been employed. This final form of the transformed set of governing equations are solved numerically, and the method is described in the next chapter.

CHAPTER III

METHOD OF SOLUTION

III.A. FINITE DIFFERENCE EQUATIONS

In order to solve Eqs. (II-55) to (II-58) and Eq. (II-60), which form a set of coupled nonlinear partial differential equations, each equation is first transformed into the finite difference form. Implicit method was employed to obtain the finite difference form of three equations. Thus, a spatial partial derivative is approximated by finite difference terms evaluated at the advanced time τ_{n+1}. The transformation is achieved by establishing a network of grids throughout the region $0 \leq \eta \leq \eta_{max}$, and $0 \leq \tau \leq \tau_{max}$ with grid spacings $\Delta\eta$ and $\Delta\tau$ respectively (see Fig. 5). Fig. 6 shows schematically the grid points involved in the space and time difference approximations used in the analysis. At any grid point denoted by (i,n), the finite difference form of the governing equations can be represented by the general equation

$$-A_i Z_{(i-1,n+1)} + B_i Z_{(i,n+1)} - C_i Z_{(i+1,n+1)} = D_{(i,n)}, \qquad 2 \leq i \leq M \qquad \text{(III-1)}$$

At any one time level τ_n, Eq. (III-1) will be written once for each grid point $2 \leq i \leq M$. This results in a system of $(M-1)$ simultaneous equations with $(M-1)$ unknown variables in

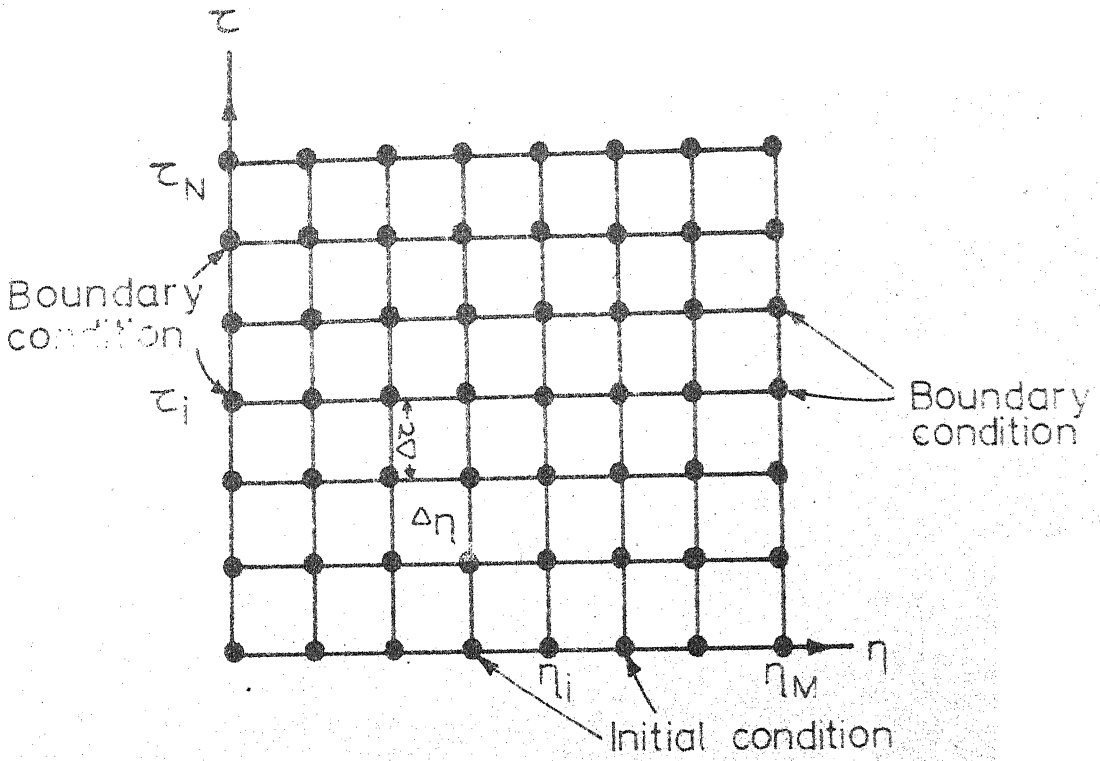

FIG. 5 – ARRANGEMENT OF GRID POINTS FOR DIFFERENCE EQUATIONS

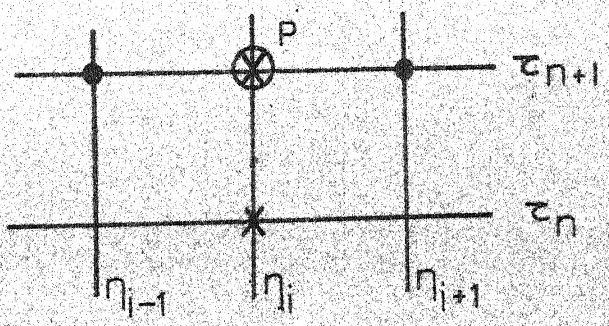

FIG. 6 – IMPLICIT FORM OF FINITE DIFFERENCE MESH.

$Z_{(i,n+1)}$. Before going into the method of solution of such a system we will obtain the finite difference form of the governing equations.

Since Eqs. (II-55) and (II-58) are nonlinear equations, the nonlinear terms are linearized in the following manner.

Consider a nonlinear function $G(g_1,g_2,\ldots,g_N)$ of several dependent variables like $g_1,g_2,\ldots,g_N$. This function can be expanded in a Taylor's series about a value of g_i either guessed or known from previous iteration. That is,

$$G(g_1,g_2,\ldots,g_N)^{(k+1)} = [G(g_1,g_2,\ldots,g_N)]^{(k)} + \sum_{j=1}^{N} \left(\frac{\partial G}{\partial g_j}\right)^{(k)} (g_i^{(k+1)} - g_i^{(k)}) \qquad \text{(III-2)}$$

where k represents iteration number for evaluation of G. Note that as soon as $g_i^{(k+1)}$ becomes equal to $g_i^{(k)}$ within a prescribed limit, $G^{(k+1)}$ and $G^{(k)}$ also become equal to that accuracy.

With the help of Eq. (III-2), the nonlinear terms of Eqs. (II-55) and (II-58) can be expressed as follows:

$$[p_{(i,n+1)}^{(k+1)}]^2 = [p_{(i,n+1)}^{(k)}][2p_{(i,n+1)}^{(k+1)} - p_{(i,n+1)}^{(k)}] \qquad \text{(III-3)}$$

$$\left[\frac{\exp\{-\varepsilon/\theta_{(i,n+1)}\}}{\theta_{(i,n+1)}^{n_o-1}}\right]^{(k+1)} = a_{(i,n+1)}^{(k)} + b_{(i,n+1)}^{(k)}\,\theta_{(i,n+1)}^{(k+1)} \qquad \text{(III-4)}$$

where $a^{(k)}_{(i,n+1)} = \dfrac{\exp\{-\varepsilon/\theta^{(k)}_{(i,n+1)}\}}{[\theta^{(k)}_{(i,n+1)}]^{n_o}} [n_o\theta^{(k)}_{(i,n+1)} - \varepsilon]$, (III-5)

and $b^{(k)}_{(i,n+1)} = \dfrac{\exp\{-\varepsilon/\theta^{(k)}_{(i,n+1)}\}}{[\theta^{(k)}_{(i,n+1)}]^{n_o+1}} [\varepsilon + (1-n_o)\theta^{(k)}_{(i,n+1)}]$ (III-6)

The various derivatives in the governing equations have been approximated by finite difference expressions as described below.

The first order derivatives with respect to η like p', Y_F', Y_O', θ' and θ_ℓ' are approximated by the central difference formula. That is,

$$[p']^{(k+1)}_{(i,n+1)} = [p^{(k+1)}_{(i+1,n+1)} - p^{(k+1)}_{(i-1,n+1)}]/2h \text{ , etc.} \quad \text{(III-7)}$$

Similarly, for p'', Y_F'', Y_O'', θ'' and θ_ℓ'', the following three point difference approximation is used,

$$[p'']^{(k+1)}_{(i,n+1)} = [p^{(k+1)}_{(i+1,n+1)} - 2p^{(k+1)}_{(i,n+1)} + p^{(k+1)}_{(i-1,n+1)}]/h^2, \quad \text{etc.} \quad \text{(III-8)}$$

To express the time derivatives, $(\partial p/\partial\tau)$, etc., in difference form, the backward difference scheme is used as given below,

$$\left(\frac{\partial p}{\partial \tau}\right)^{(k+1)}_{(i,n+1)} = \left[\frac{p^{(k+1)}_{(i,n+1)} - p_{(i,n)}}{\Delta\tau}\right] \text{ , etc.} \quad \text{(III-9)}$$

Note that the quantities already known at the previous time-step do not require any iteration index. In order to evaluate the first order derivatives of the dependent variables at the droplet surface which appear in the interface conditions, slightly more accurate three point difference formulae have been used. That is,

$$[Y_O']^{(k+1)}_{(1,n+1)} = \frac{1}{2h}\left[4Y_{O(2,n+1)}^{(k+1)} - Y_{O(3,n+1)}^{(k+1)} - 3Y_{O(1,n+1)}^{(k+1)}\right] \quad \text{(III-10)}$$

$$[Y_F']^{(k+1)}_{(1,n+1)} = \frac{1}{2h}\left[4Y_{F(2,n+1)}^{(k+1)} - Y_{F(3,n+1)}^{(k+1)} - 3Y_{F(1,n+1)}^{(k+1)}\right] \quad \text{(III-11)}$$

$$[\theta']^{(k+1)}_{(1,n+1)} = \frac{1}{2h}\left[4\theta_{(2,n+1)}^{(k+1)} - \theta_{(3,n+1)}^{(k+1)} - 3\theta_{(1,n+1)}^{(k+1)}\right] \quad \text{(III-12)}$$

$$[\theta_\ell']^{(k+1)}_{(1,n+1)} = \frac{1}{2h}\left[4\theta_{\ell(2,n+1)}^{(k+1)} - \theta_{\ell(3,n+1)}^{(k+1)} - 3\theta_{\ell(1,n+1)}^{(k+1)}\right] \quad \text{(III-13)}$$

Therefore Eqs. (II-55) to (II-58), and Eq. (II-60) are now readily transformed into the following set of linear finite difference equations:

$$-r\left[C - (h/2)f_{(i,n+1)}^{(k)}\right]p_{(i-1,n+1)}^{(k+1)} + \left[1 + 2rC + 2rh^2\, p_{(i,n+1)}^{(k)}\right]p_{(i,n+1)}^{(k+1)}$$

$$-r\left[C + (h/2)f_{(i,n+1)}^{(k)}\right]p_{(i+1,n+1)}^{(k+1)}$$

$$= p_{(i,n)} + \left[\theta_{(i,n+1)}^{(k)} + \{p_{(i,n+1)}^{(k)}\}^2\right]rh^2 \quad \text{(III-14)}$$

$$-r[C/Sc - (h/2)\, f_{(i,n+1)}]\, Y_{F_{(i-1,n+1)}}^{(k+1)}$$

$$+ [1 + 2rC/Sc + \frac{\nu_F W_F r h^2 K(Y_{O_{(i,n+1)}}^{(k)}) \exp\{-\varepsilon/\theta_{(i,n+1)}^{(k)}\}}{\theta_{(i,n+1)}^{(k)}}]\, Y_{F(i,n+1)}^{(k+1)}$$

$$-r[C/Sc + (h/2)\, f_{(i,n+1)}]\, Y_{F_{(i+1,n+1)}}^{(k+1)} = Y_{F_{(i,n)}} \qquad \text{(III-15)}$$

$$-r[C/Sc - h/2\, f_{(i,n+1)}]\, Y_{O_{(i-1,n+1)}}^{(k+1)}$$

$$+ [1 + 2rC/Sc + \frac{\nu_O W_O r h^2 K(Y_{F_{(i,n+1)}}) \exp\{-\varepsilon/\theta_{(i,n+1)}^{(k)}\}}{\theta_{(i,n+1)}^{(k)}}]\, Y_{O(i,n+1)}^{(k+1)}$$

$$-r[C/Sc + (h/2)\, f_{(i,n+1)}]\, Y_{O_{(i+1,n+1)}}^{(k+1)} = Y_{O_{(i,n)}} \qquad \text{(III-16)}$$

$$-r[C/Pr - h/2\, f_{(i,n+1)}]\, \theta_{(i-1,n+1)}^{(k+1)}$$

$$+ [1 + 2rC/Pr - \nu_F W_F r h^2 KQ\, b_{(i,n+1)}^{(k)}\, Y_{O_{(i,n+1)}}\, Y_{F_{(i,n+1)}}]\theta_{(i,n+1)}^{(k+1)}$$

$$-r[C/Pr + (h/2)\, f_{(i,n+1)}]\, \theta_{(i+1,n+1)}^{(k+1)}$$

$$= \theta_{(i,n)} + r h^2 KQ\, a_{(i,n+1)}^{(k)}\, Y_{O_{(i,n+1)}}\, Y_{F_{(i,n+1)}} \qquad \text{(III-17)}$$

$$-r\left[1 + f_s(h/2)\frac{C_\ell}{C_p\varphi^{\frac{1}{2}}}\right]\theta_{\ell_{(i-1,n+1)}} + [1 + 2r]\,\theta_{\ell_{(i,n+1)}}$$

$$-r\left[1 - f_s(h/2)\frac{C_\ell}{C_p\varphi^{\frac{1}{2}}}\right]\theta_{\ell_{(i+1,n+1)}} = \theta_{\ell_{(i,n)}} \qquad \text{(III-18)}$$

where

$$r = \frac{\Delta\tau}{h^2} \quad \text{and} \quad K = (At_f/\ \rho_e^{-1}W_O W_F) \qquad \text{(III-19)}$$

We have assumed here an over-all single step second order chemical reaction between the fuel and the oxidizer vapours.

The interface conditions stated in Eqs. (II-66) to (II-68) with the help of Eqs. (III-10) to (III-13) become

At the droplet surface $\eta = 0$:

$$p_{(1,n+1)} = 0 \qquad \text{(III-20)}$$

$$Y_{F_{(1,n+1)}}^{(k+1)} = Y_{F,s} = \frac{[4Y_{F_{(2,n+1)}}^{(k+1)} - Y_{F_{(3,n+1)}}^{(k+1)} - 2hf_s]}{(3 - 2hf_s)} \qquad \text{(III-21)}$$

$$Y_{O_{(1,n+1)}}^{(k+1)} = Y_{O,s} = \frac{[4Y_{O_{(2,n+1)}}^{(k+1)} - Y_{O_{(3,n+1)}}^{(k+1)}]}{(3 - 2hf_s)} \qquad \text{(III-22)}$$

$$\theta_{(1,n+1)}^{(k+1)} = \theta_s$$

$$\frac{4[\theta_{(2,n+1)}^{(k+1)} + \varphi^{\frac{1}{2}}\theta_{\ell_{(2,n+1)}}^{(k+1)}] - [\theta_{(3,n+1)}^{(k+1)} + \varphi^{\frac{1}{2}}\theta_{\ell_{(3,n+1)}}^{(k+1)}] + [2hQ_{vap}]}{3[1 + \varphi^{\frac{1}{2}}]} \qquad \text{(III-23)}$$

And, at the edge of the boundary layer, $\eta \longrightarrow \infty$:

$$p_{(M+1,n+1)} = 1, \quad Y_{O_{(M+1,n+1)}} = Y_{O,e}, \quad Y_{F_{(M+1,n+1)}} = 0,$$

$$\theta_{(M+1,n+1)} = 1 \qquad \text{(III-24)}$$

The numerical procedure of solving the finite difference equations, Eqs. (III-14) to (III-24) is described in the next section.

III.B SOLUTION TO THE FINITE DIFFERENCE EQUATIONS

As already mentioned each of the finite difference equations, namely Eqs. (III-14) to (III-18) can be represented in the general form of Eq. (III-1). As a result (M-1) linear equations will be obtained at each time step. These equations can be represented in the form of square tridiagonal matrix of coefficients A_i, B_i and C_i. The right hand side of these equations, D_i is a known quantity. Therefore, with the help of appropriate boundary conditions, solutions to these tridiagonal system of equations can be readily obtained by Gaussian elimination technique (26). This technique is computationally stable for a vast choice of step sizes and has outweighed the moderate increase in computational effort when compared to the other techniques. Numerical computations were done by programming in Fortran on IBM 7044/1401 digital computers. The following important points must be kept in mind before

proceeding for computation.

As already mentioned in Section III.A, the implicit difference scheme involves the computation of values at an advanced time step, τ_{n+1}, making use of the evaluated values at the previous time step τ_n. Since the droplet is injected instantaneously, there will be sharp gradients in the flow variables at $\tau = 0$. However, the numerical treatment is made possible by starting integration after a very small interval of time. The initial values for quantities like p, Y_F, Y_O, θ_ℓ and θ are calculated from the functions developed for the integral technique in reference 24. A reasonable guess for τ ($\tau = 10^{-3}$) was made to startwith. Initial guess was made for mass fraction of species ($Y_{O,s}$ and $Y_{F,s}$), and f_s at the interface.

Stable solutions were found out for each of the profiles f, p, θ_ℓ, Y_O, Y_F and θ, by solving the finite differenc equations simultaneously. In obtaining the solution the wall values are assumed at first and then checked with the boundary conditions expressed by three point difference formulae. For example, Eq. (III-23) was used to obtain refined interface temperature (θ_s). The process is repeated till all the interface values converge to the desired accuracy. As soon as the new profiles were obtained old ones were replaced by them in order to compute for the next time step. The iteration procedure was repeated until a prescribed convergence of

1 in 1000 was obtained for all the required quantities.

In order to advance the solution in time, a small increment in the time step ($\Delta\tau$) was given. The solutions obtained at the previous time step were used as the input profiles for the next time step. The same procedure is repeated as described in the previous section until a converged solution is obtained at this τ-values. The computations are stopped when the field variables reach steady state. It was found convenient to use a variable time step. Time steps of 10^{-3} to 10^{-1} were used for the unsteady part of the solution.

Asymptotic approach of the profiles p, Y_O, Y_F, θ and θ_ℓ was obtained by trying various values of η_{max}. An optimum choice of $\eta_{max} = 8$ was found adequate to satisfy the external flow conditions.

CHAPTER IV

RESULTS, DISCUSSIONS AND CONCLUSIONS

IV.A RESULTS AND DISCUSSIONS

The computations for transient combustion of a fuel under forced convective conditions was undertaken to determine the time scales characterizing the various physical processes involved in it. The numerical values of the physical constants appearing in the governing equations are chosen to correspond to those of stable liquid pentaborane (B_5H_9). As compared to many hydrocarbon fuels, pentaborane is chemically more active, has a high calorific value and is stable over a larger period during storage (27). For poorly known values of some physical constants, a set of different values were tried. In addition, the values of certain parameters were varied in order to study their effect on the combustion process. A list of the data used in the numerical calculations is given in Appendix I. Each case there refers to a set of input data for one complete solution.

Detailed profiles of velocity (p'), species mass-fractions (Y_O and Y_F), and temperatures (θ and θ_ℓ) as a function of τ and η are shown respectively in Figs. 7 to 11 for one set of physical data (case I of Appendix I). It is evident from these figures that the gaseous boundary layer

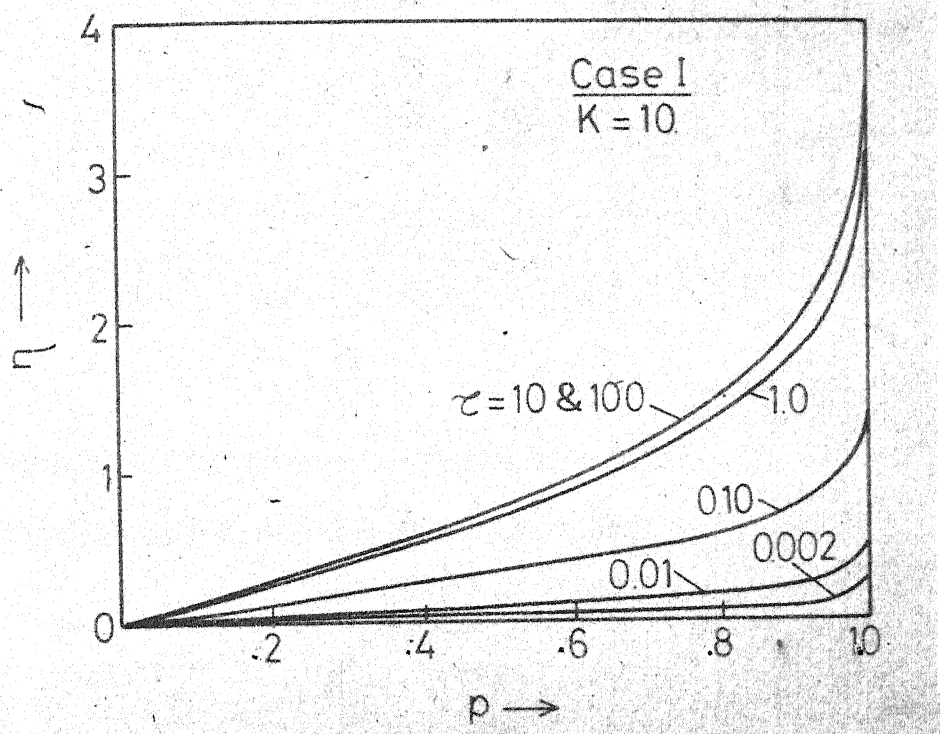

FIG. 7. VELOCITY PROFILES AT DIFFERENT TIME INTERVALS

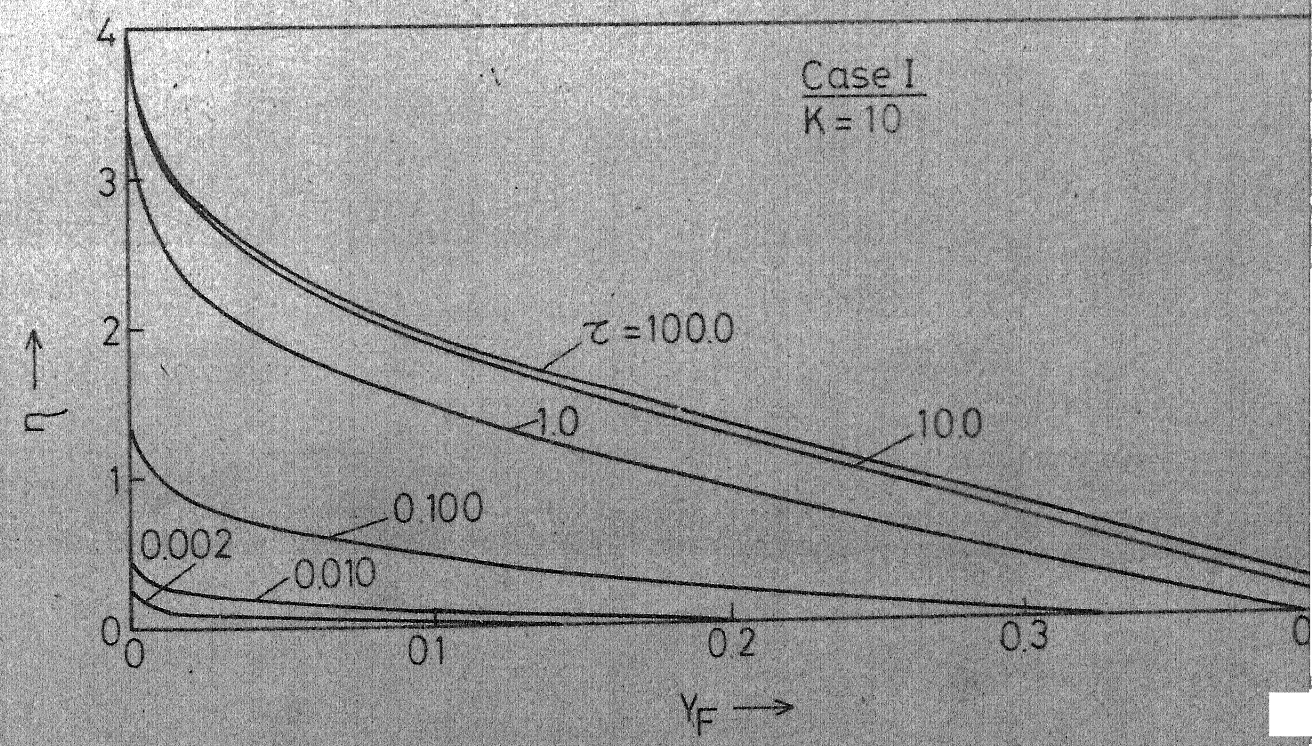

FIG. 8. MASS FRACTION PROFILES OF FUEL AT DIFFERENT TIME INTERVALS.

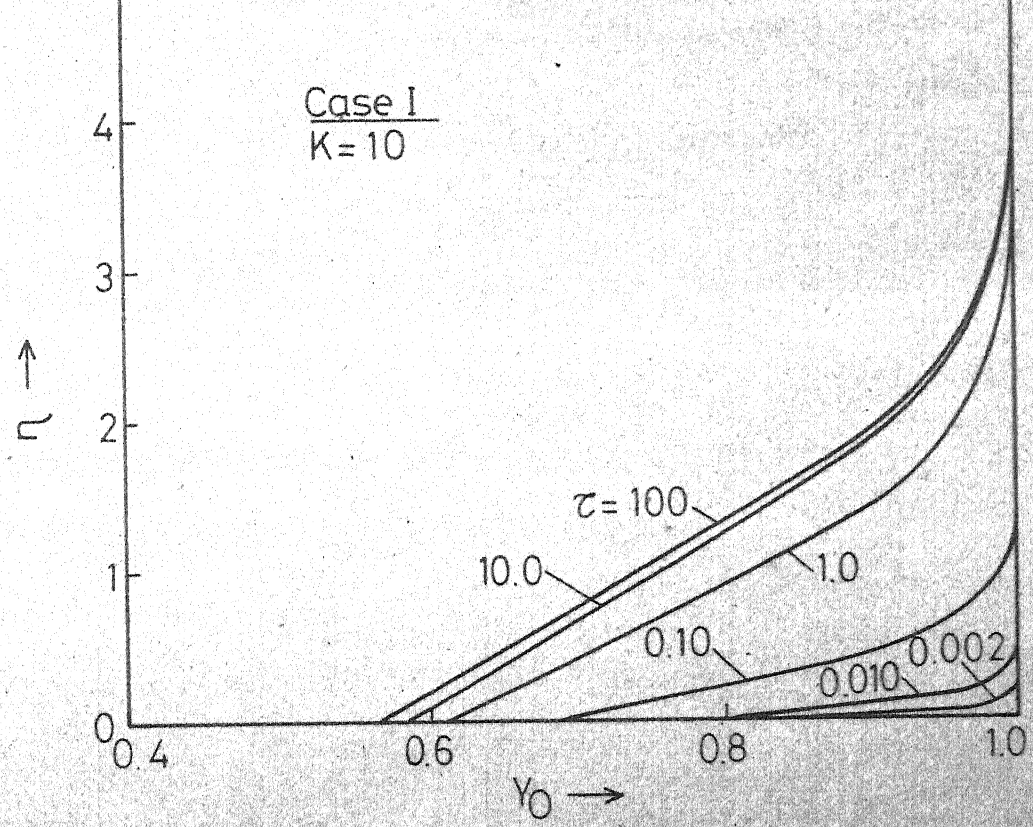

FIG.9. MASS FRACTION PROFILES OF OXIDIZER AT DIFFEREN TIME INTERVALS.

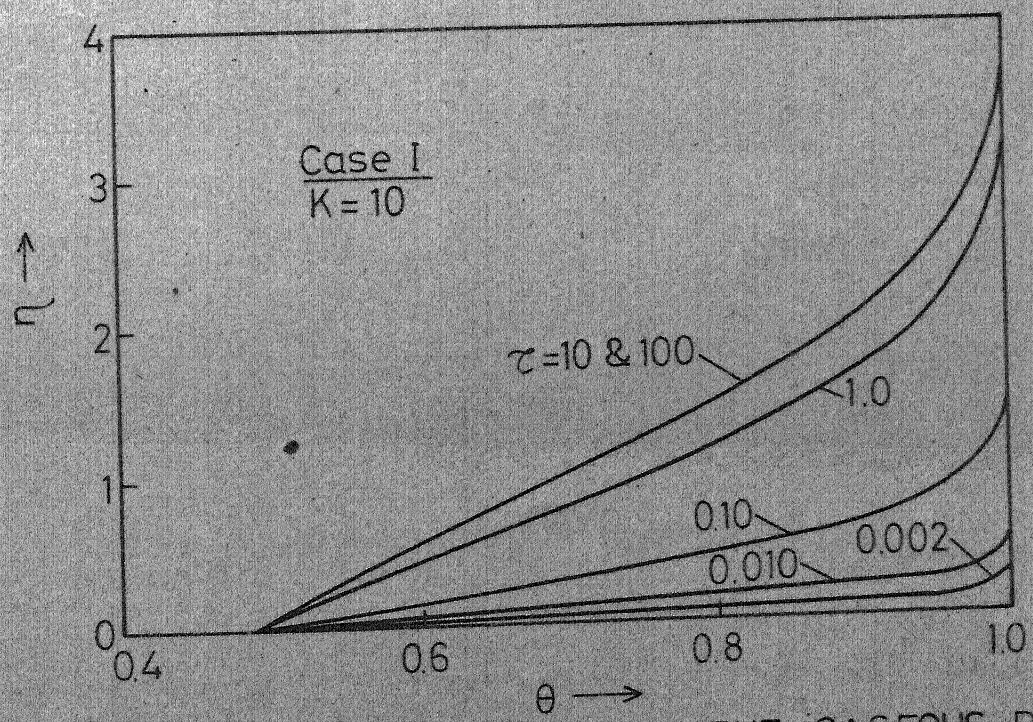

FIG.10. TEMPARATURE PROFILES IN THE GASEOUS PHASE A DIFFERENT TIME INTERVALS.

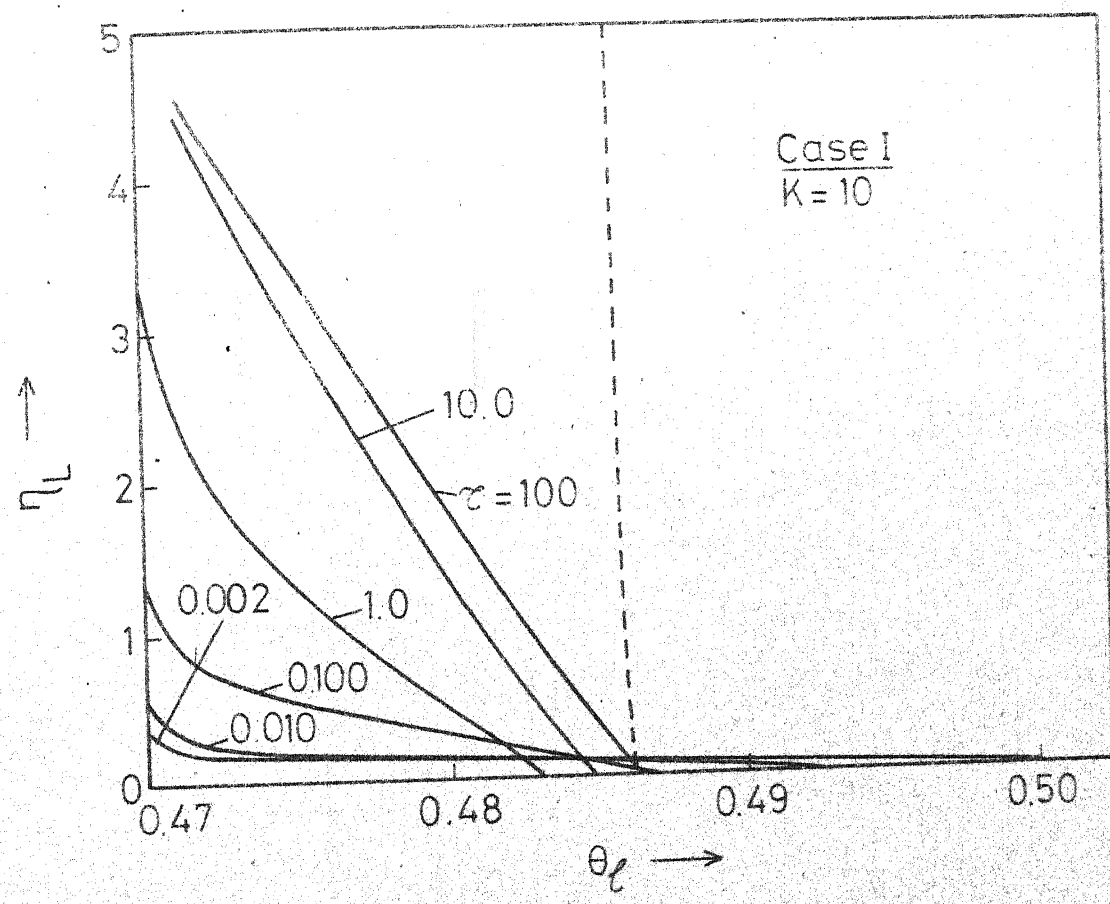

FIG.11. LIQUID PHASE TEMPERATURE PROFILES AT DIFFERENT TIME INTERVALS.

grows with passage of time until the steady state profiles are obtained. In fact the viscous boundary layer thickness does not change as soon as τ becomes of the order of unity which is reasonable since the characteristic flow time is taken equal to t_f. The velocity and temperature profiles (Figs. 7 and 10) attain steady state behaviour at about $\tau = 10$ while the species mass fractions profiles (Figs. 8 and 9) do so around $\tau = 100$. In otherwords, as expected the detailed behaviour of the gaseous boundary layer is controlled by the species diffusion rates, before the gaseous phase attains a quasi-steady state behaviour. As τ increases, the thermal layer thickness in the liquid fuel goes on increasing in an asymptotic manner which requires more computing time with a variable $(\eta_\ell)_{max}$. However, using the steady-state constant values for f_s and θ_s, it is possible to obtain the steady-state temperature distribution in the liquid fuel with the help of Eqs. (II-60) to (II.63). The result is shown by a dotted curve in Fig. 11. It is clear that the temperature distribution obtained from the unsteady equations does not attain steady-state results even when $\tau = 100$, unlike the processes in the gaseous phase. Thus, the wet bulb temperature is not achieved at the liquid fuel surface. It is therefore important to note that the vaporization kinetics controls the unsteady combustion of the fuel.

It is also instructive to study the behaviour of the variables at the gas-liquid interface. Fig. 12 shows the

variation of the vaporization rate ($- f_s$), the interface fuel mass fraction ($Y_{F,s}$), and the interface temperature (θ_s) with time (τ). The interface temperature remains practically constant. However, it must be pointed out that even a slight variation in its magnitude results in a significant change in the vaporization rate because of the exponential dependence in the kinetic terms. It has been assumed in the present analyses that there are no fuel vapours initially in the surrounding environment when the droplet is injected into it. Consequently, the vaporization rate must be high at the initial stages such that the liquid provides a part of its own latent heat of vaporization which results in a slight decrease in the magnitude of the interface temperature. The starting values of both the fuel vapour pressure $(Y_{F,s})_{eq.}$ and the evaporation rate ($- f_s$) are determined by the initial value of the interface temperature (θ_s) which is chosen to be between unit and $\theta_{\ell,o}$. Note that $Y_{F,s}$ will be close to zero at the initial stage because there will be hardly any fuel loading into the gaseous boundary layer. However, $Y_{F,s}$ starts building up as time increases (see Fig. 12). As τ approaches unity, the boundary layer growth becomes steady as described previously but, from Fig. 12, we find that the interface temperature begins to increase which results in a slight increase in $-f_s$ and $Y_{F,s}$. At τ equal to about 50, interface temperature ceases to increase, and remains constant afterwards. Instead, $Y_{F,s}$ keeps on increasing

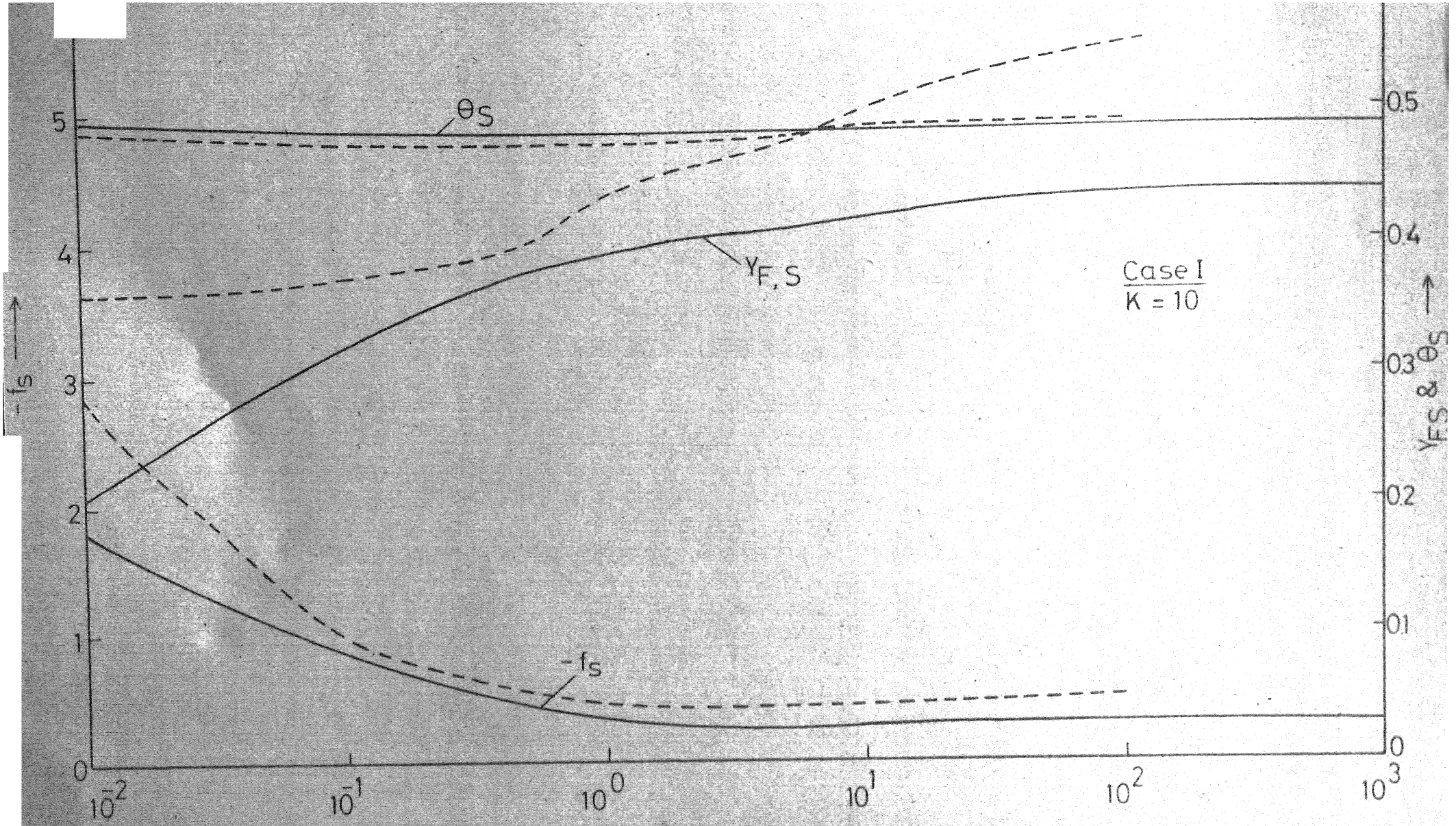

FIG.12. VARIATION OF INTERFACE FUEL MASS FRACTION ($Y_{F,S}$) AND INTERFACE TEMPARATURE (T_S) WITH TIME (τ). DOTTED CURVE REPRESENT THE CALCULATION BASED ON INTEGRAL METHOD (24).

till τ is around 100. Thus the interface fuel mass fraction does not respond instantaneously to the increased vaporization rate, and there is certain time lag within which $Y_{F,s}$ builds up corresponding to the new vaporization rate.

Results of the computations based on an integral method (24) are shown by dotted curves in Fig. 12. There is an appreciable difference in the absolute values of the different variables. Also, there is a substantial loading of fuel at the initial stage unlike the results of the present computations.

Next we have obtained complete solutions by varying the temperature of the oxidizer stream (T_e) and the evaporation kinetic parameter (ϵ) to estimate their effect on combustion process. The general behaviour of the detailed profiles for f', Y_O, Y_F, θ, and θ_ℓ were found to be very similar to those obtained for case I.

The effect of increasing the temperature of the external stream (T_e) on the interface parameters is shown in Fig. 13. Here the data corresponds to case II in Appendix I. The surface temperature behaviour is very similar to the one observed in case I (see Fig. 12). There occurs a substantial increase in the vaporization rate as well as the interface fuel mass fraction compared to the previous case.

The effect of decreasing the magnitude of evaporation constant (ϵ) on the variables at the interface is shown in Fig. 14 corresponding to the data of case III in Appendix I.

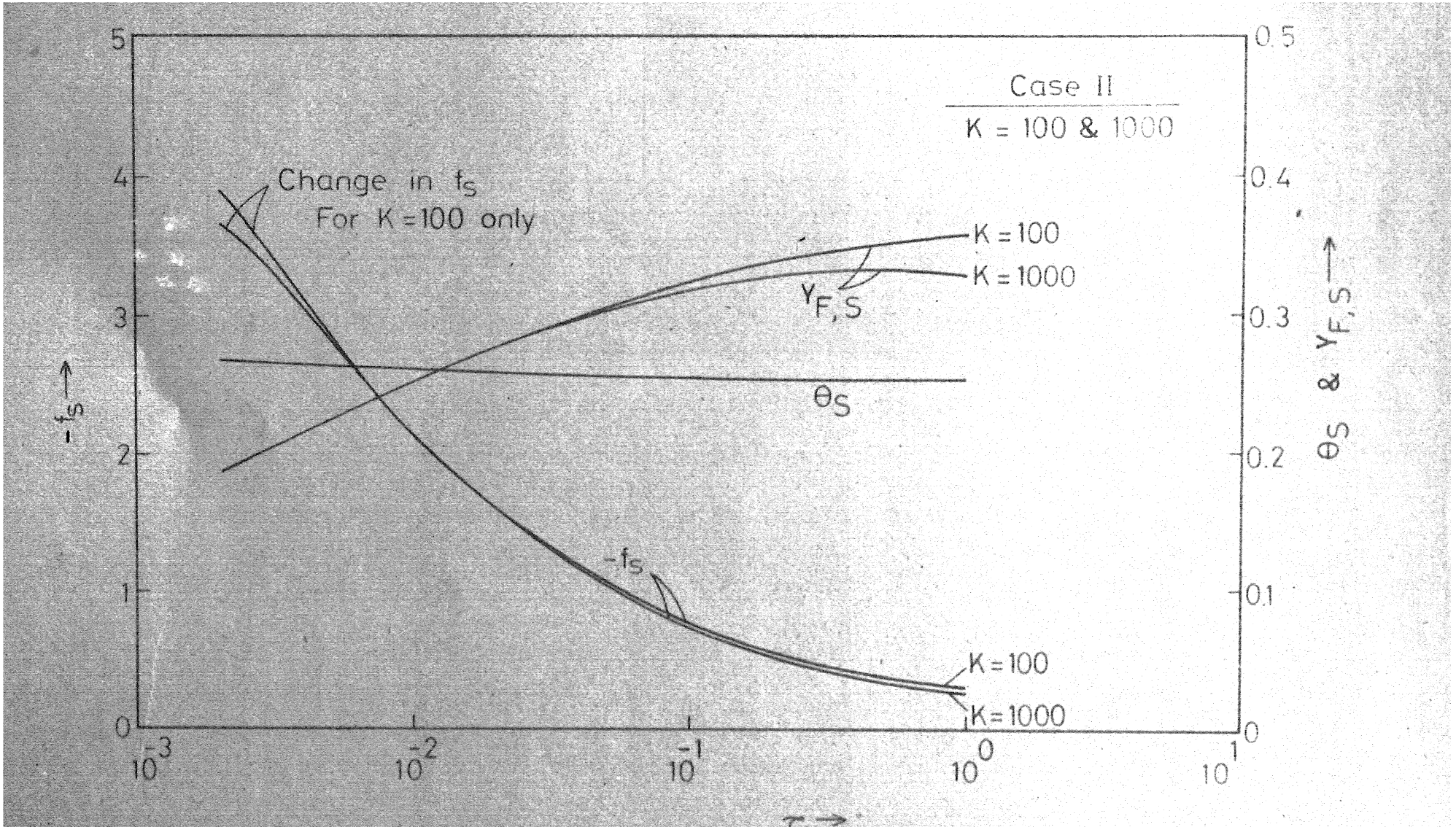

FIG 13 EFFECT OF INCREASING EXTERNAL STREAM TEMPARATURE (T_e) ON INTERFACE PARAMETERS.

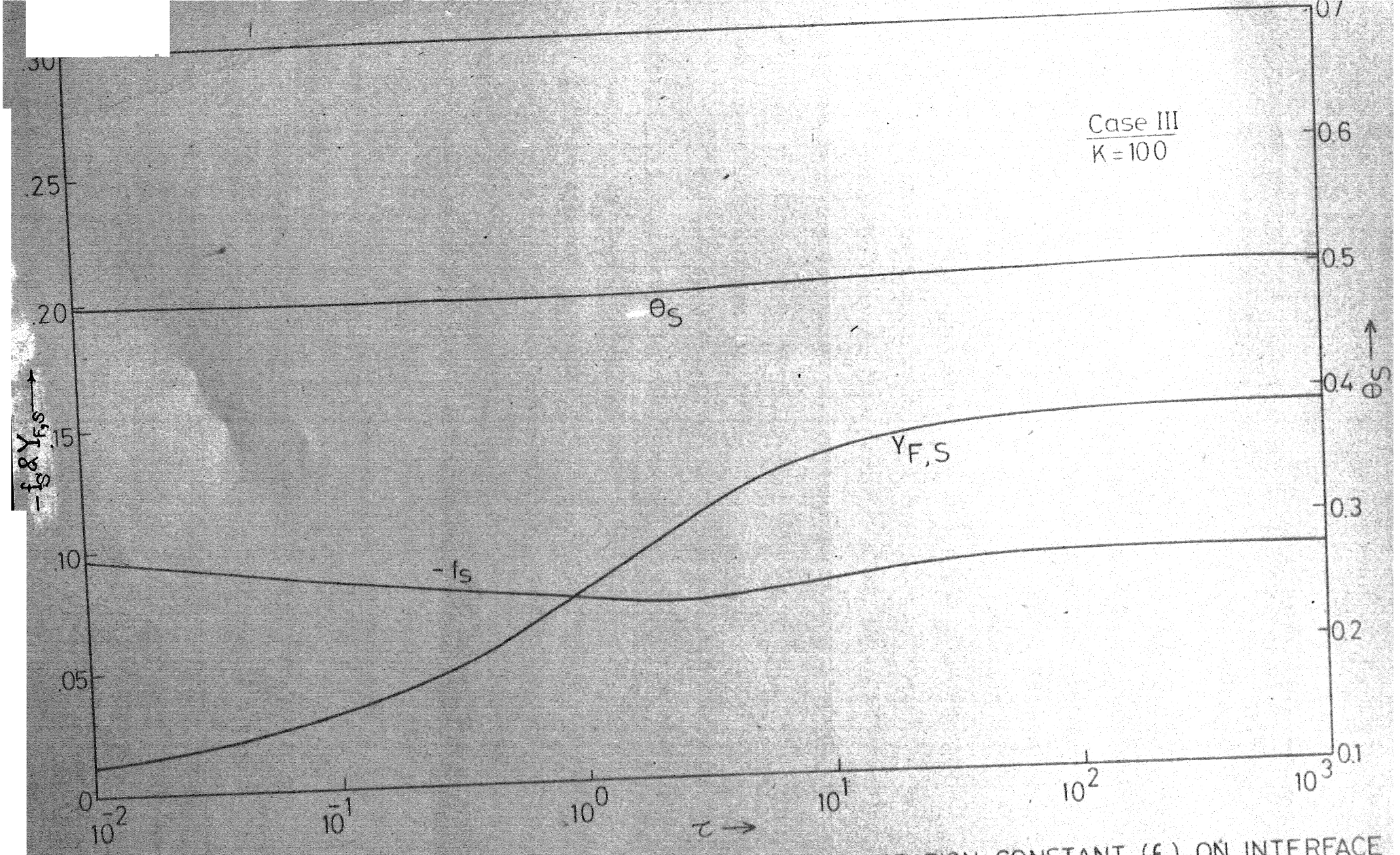

FIG.14. EFFECT OF DECREASING THE MAGNITUDE OF EVAPORATION CONSTANT (ε) ON INTERFACE PARAMETERS.

There occurs a pronounced reduction in the vaporization rate as well as in the fuel mass fraction at the surface. However, the interface temperature remains almost the same in magnitude as well as behaviour as in case I. At about $\tau = 2$ we find that vaporization rate has started increasing due to the increase in interface temperature in a manner similar to case I. However the overall effect is more pronounced here because of the fact that there is a reduction in the absolute values during the initial time period. Also, it is interesting to note that the decreased evaporation constant, ϵ, has also reduced the time lag between the building up of $Y_{F,s}$ with the corresponding vaporization rate.

The combined effect of slow vaporization kinetics and increased external stream temperature on the interface parameters is shown in Fig. 15 corresponding to the data of case IV in Appendix I. Like case III, the slow kinetics has reduced vaporization rate substantially as compared to case I and thus delaying the building up of fuel mass fraction inside the gaseous boundary layer. Also, as observed earlier higher external stream temperature increases the interface temperature. This indicates clearly that vaporization kinetics is an important factor in determining the vaporization rate. Around $\tau = 2$ the interface temperature begins to rise more rapidly resulting in higher values of the vaporization rate as well as fuel mass fraction. It appears that significant chemical

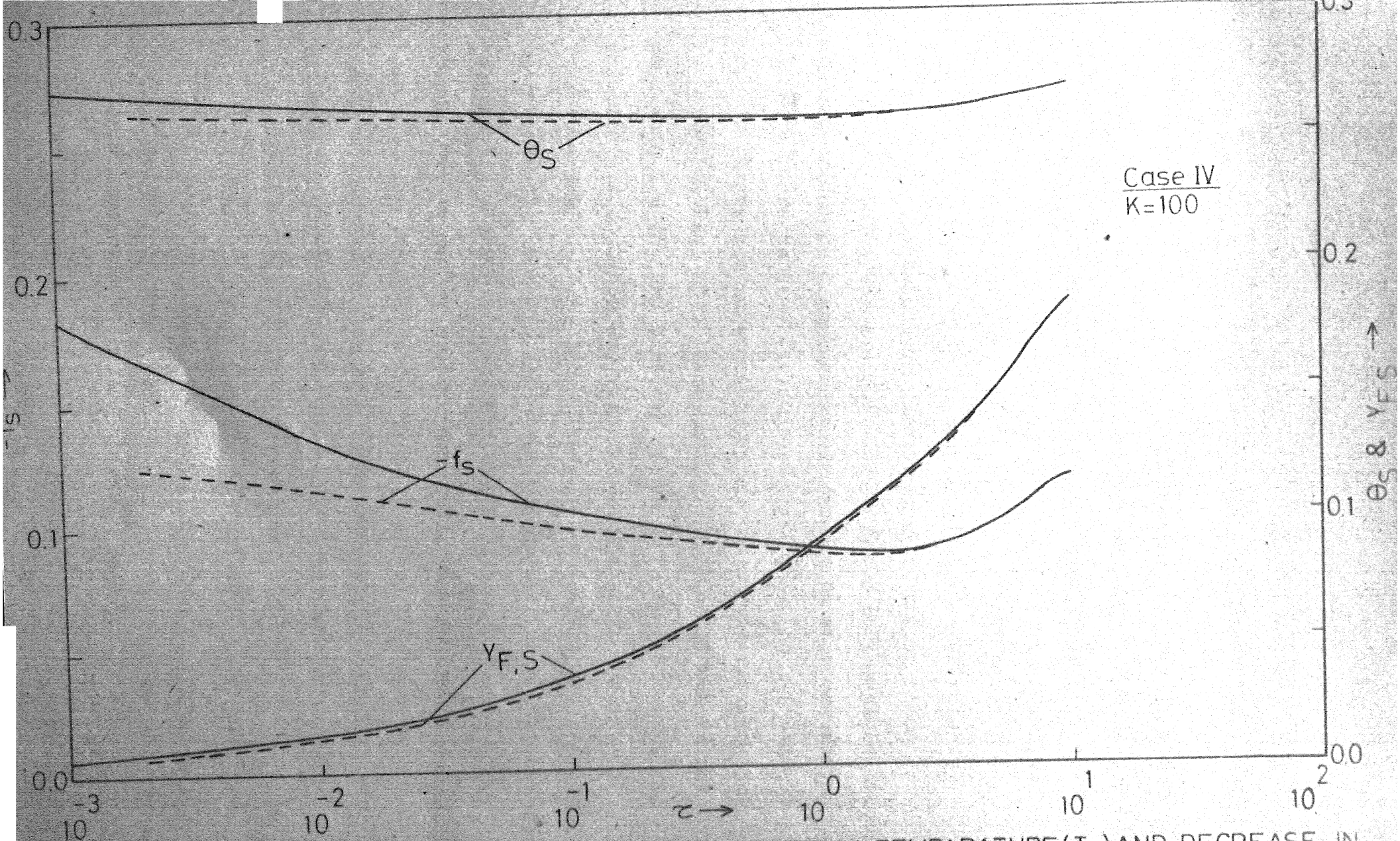

FIG.15. COMBINED EFFECT OF INCREASE IN EXTERNAL STREAM TEMPARATURE (T_e) AND DECREASE IN EVAPORATION CONSTANT (ϵ) ON INTERFACE PARAMETERS. DOTTED CURVES ARE FOR A DIFFERENT CHOICE OF INTERFACE TEMPARATURE.

activity resulting in an additional source of heat rises the interface temperature after sometime. At around $\tau = 10$ boiling point of the liquid is reached and the calculations continued for the next time intervals showed that equilibrium fuel mass fractions were greater than unity. The present analysis then breaks down for further calculations.

The effect of variation in the relative velocity of hot external stream was also studied by varying the parameter K. The values of K used in these computations are 10, 100, and 1000. An increase in the value of K actually means an increase in the flow residence time (or low values of U_e). There was no significant change in the results (see, for example, Fig. 13). Computations for case II were also done when K = 10, and here the increase in free stream velocity did not show any significant change in the values like vaporization rate and interface temperature as compared to the results when K = 100. But a decreased free stream velocity (K = 1000) showed that the fuel loading inside the boundary layer was of smaller magnitude when compared to the case when K = 100. This difference in the two cases considered can be attributed to the high relative velocity which exists between the droplet and the surrounding hot stream resulting in sweeping out more fuel by convection effects.

The effect of a choice for initial values of

interface temperature (θ_s) is significant in the initial stages, but it did not bring any substantial change as far as the steady state behaviour is concerned. Similarly the effect of initial selection for vaporization rate to start the numerical solution was also studied. In Fig. 13 the effect of initial guess is also shown. Since no appreciable change was found either in the interface temperature or in the surface fuel mass fraction development with time or in the final steady state values, it was concluded that the initial guess can be made somewhat arbitrarily.

Before concluding the discussion of the results of computations it is useful to discuss the time scales which could play an important role in the phenomena of combustion instability. As mentioned already in Chapter I the unsteady interactions can occur if the energy addition is in phase with the flow disturbance. In other words, if the product of the characteristic time of the combustion process (t_c) and angular frequency (ω) of the acoustic oscillation is of the order of unity. A typical estimate is made by considering a droplet of radius 100 microns injected into a free oxidizing stream having a relative velocity of 25 m/sec. Then the characteristic flow time t_f will be of the order of 4×10^{-6} sec. Making use of the time scale at which gaseous phenomena has attained steady state (i.e. $\tau = 100$), the unsteady interactions with the gas phase can occur provided that the circular frequency

of the acoustic oscillation is of the same order as that of $1/t_c$. That is, if ω is of the order of 2500 Hz. In general, the fuel spray consists of droplets with varying sizes and having somewhat different velocities. Consequently, several other values of acoustic frequencies may come into play when the combustion instability problem is analyzed in detail for a rocket motor chamber.

IV.B CONCLUSIONS

Detailed profiles for velocity, species mass fractions, and temperature have been obtained for pentaborane droplets. In order to investigate the transient burning of a droplet, it is essential to take into account non-equilibrium vaporization kinetics since the steady state situation is not obtained for the thermal behaviour within the liquid droplet while the gaseous phase phenomena becomes steady much earlier. However, the analysis for a droplet burning can be treated as a quasi-steady phenomena after a time greater than an order of magnitude of the characteristic flow time.

LIST OF REFERENCES

1 Ranz, W.E., and Marshall, Jr., W.A., 'Evaporation from Drops - Part I', Chem. Eng. Prog. 48 (3), 141-146 (1952). Also, 'Evaporation from Drops - Part II', Chem. Eng. Prog. 48 (4), 173-180 (1950).

2 Spalding, D.B., 'Combustion of Liquid Fuel in a Gas Stream - I Fuel 29, 2-7 (1950). Also, 'Combustion of Liquid Fuel in a Gas Stream - II', Fuel 29, 25-32 (1950).

3 Spalding, D.B., 'Experiments on the Burning and Extinction of Liquid Fuel Spheres', Fuel 32, 169-185 (1953). Also, 'The Combustion of Liquid Fuels', Fourth Symposium (International) on Combustion, Williams and Wilkins Co. Baltimore, U.S.A., pp 847-864 (1953).

4 Godsave, G.A.E., 'Studies of the Combustion of Drops in a Fuel Spray - The Burning of Single Drops of Fuel', Fourth Symposium (International) on Combustion, Williams and Wilkins Co. Baltimore, U.S.A., pp 818-830 (1953).

5 Penner, S.S., and Goldsmith, M., 'On the Burning of Single Drops of Fuel in an Oxidizing Atmosphere', Jet Propulsion 24, 245-251 (1954).

6 Lorell, J., Wise, H., and Carr, R.E., 'Steady-State Burning of a Liquid Droplet II. Bipropellant Flame', J. Chem. Phys. 25, 325-331 (1956).

7 Wise, H., and Agoston, G.A., 'Literature of the Combustion of Petroleum', American Chemical Society, Washington, D.C. (1958).

8 Williams, F.A., 'Combustion Theory', Addison-Wesley Publishing Company, Inc., London (1965).

9 Gohrbandt, W., N.G.T.E. Memorandum No. M. 110, April 1951.

10 Fendell, F.E., Sprankle, M.L., and Dodson, D.S., 'Thin Flame Theory for a Fuel Droplet in Slow Viscous Flow', J. Fluid. Mech. 26, 267-280 (1966).

11 Natarajan, R., and Brzustowski, T.A., 'Some New Observations on the Combustion of Hydrocarbon Droplets', Comb. Sci. Tech. 2 (4), 259-269 (1970).

12 Faeth, G.M., and Lazar, R.S., 'Fuel Droplets Burning Rates in a Combustion Gas Environment', AIAA J. 9 (11), 2165-2171 (1971).

13 Rosner, D.R., 'Liquid Propellant Rocket Combustion Instability' Eds. Harrje, D.T., and Reardon, F.H., NASA SP-194 (1972).

14 Williams, A., 'Combustion of Droplets of Liquid Fuels: A Review', Combustion and Flame 21 (1), 1-31 (1973).

15 Spalding, D.B., 'Theory of Particle Combustion at High Pressures', J. Am. Rocket Soc. 29, 828-835 (1959).

16 Rosner, D.E., 'On Liquid Droplet Combustion at High Pressures', AIAA J. 5, 163-166 (1967).

17 Chervinsky, A., 'Supercritical Burning of Liquid Droplets in Stagnant Environment', AIAA J. 7, 1815-1817 (1969).

18 Polymeropoulos, C.E., and Perkin, R.L., 'Combustion of Fuel Vapour in a Hot, Stagnant Oxidizing Environment', Comb. Sci. Tech. 5 (4), 165-174 (1972).

19 Rosner, D.E., and Chang, W.S., 'Transient Evaporation and Combustion of a Fuel Droplet near its Critical Temperature', Comb. Sci. Tech. 7 (4), 145-158 (1973).

20 Kirkaldy, I.J., 'The Time-Dependent Diffusion Theory for Condensation on Spherical and Plane Surfaces', Can J. Phys. 36, 446-455 (1958).

21 Strahle, W.C., 'A Theoretical Study of Unsteady Droplet Burning: Transients and Periodic Solutions', Department of Aeronautical Engineering, Princeton University, Princeton, New Jersey, Rep. No. 671 (1963).

22 Chervinsky, A., 'Transient Burning of Spherical Symmetric Fuel Droplets', Israel Journal of Technology 17 (1-2), 35-42 (1969).

23 Kotake, S., and Okazaki, T., 'Evaporation and Combustion of a Fuel Droplet', Int. J. Heat and Mass Transfer 12, 595-609 (1969).

24 Strahle, W.C., 'A Transient Problem on the Evaporation of a Reactive Fuel', Comb. Sci. Tech. 1, 25-33 (1969).

25 Lees, L., 'Laminar Heat Transfer Over Blunt-Nosed Bodies at Hypersonic Flight Speeds', Jet Propul. 26, 259-269 (1956).

26 Carnahan, B., Luther, H.A., and Wilkes, J.O., 'Applied Numerical Methods', John Wiley and Sons, Inc., New York (1969).

APPENDIX I

NUMERICAL DATA USED IN COMPUTATIONS

The physical values for the liquid pentaborane fuel used in the numerical computations for different cases are summarized below (28-30).

Case	T_e (^oK)	C_p at T_e (^oK) cal $mole^{-1}$ deg^{-1}	$\epsilon\sqrt{\frac{\rho t_f}{2\pi\mu_e}}$	φ	K
I	600	44.841	3.0	540	10, 100 and 1000
II	1200	65.245	3.0	1080	10, 100 and 1000
III	600	44.841	0.1	540	100
IV	1200	65.245	0.1	1080	100

C_ℓ = 36.12 cal $mole^{-1}$ deg^{-1}

E = 15,000 cal/mole

H_ℓ = 7200 cal/mole

q_r = 1085000 cal/mole

R^o = 1.987 cal/mole-^oK

$T_{\ell,o}$ = 282^oK

The non-dimensional quantities C, Pr, and Sc were simply set equal to unity. A step size equal to 0.05 was found adequate for integration in η-direction. To start the calculations in each case we chose the initial values of

$(Y_{\bar{F},s})^{\circ}_{eq}$ and $(-f_s)$ equal to 0.33, 0.1637, 0.33 and 0.1637 and -3.6, -5.7, -0.116 and -0.183 respectively.

APPENDIX II

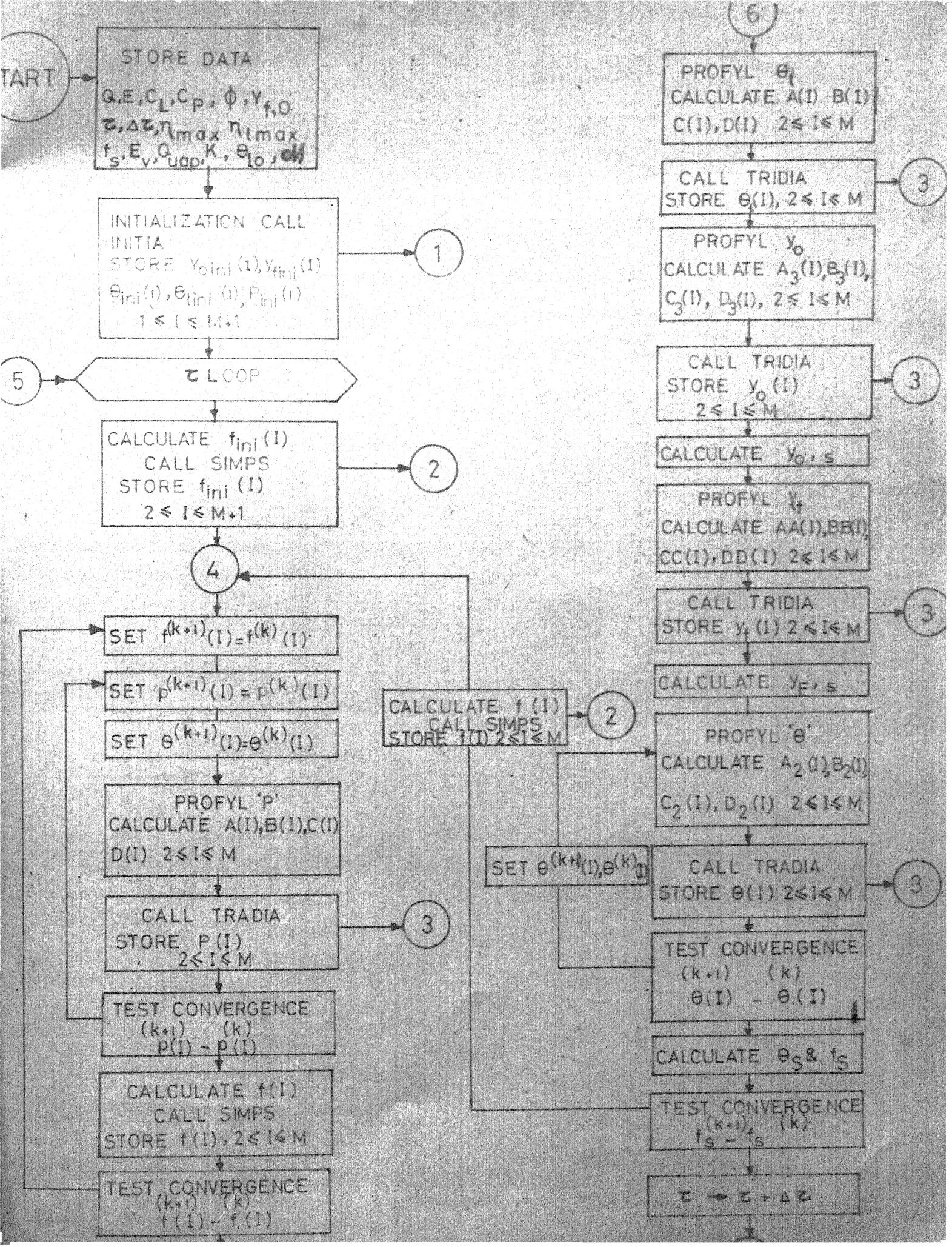
START
STORE DATA
Q, E, C_L, C_P, ϕ, $Y_{f,0}$
τ, $\Delta\tau$, η_{max} η_{max}
f_s, E_v, Q_{uap}, K, θ_{lo}, eff
INITIALIZATION CALL INITIA
STORE $Y_{oini}(I)$, $Y_{fini}(I)$
$\theta_{ini}(I)$, $\theta_{lini}(I)$, $P_{ini}(I)$
$1 \leq I \leq M+1$
1
5
τ LOOP
CALCULATE $f_{ini}(I)$
CALL SIMPS
STORE $f_{ini}(I)$
$2 \leq I \leq M+1$
2
4
SET $f^{(k+1)}(I) = f^{(k)}(I)$
SET $p^{(k+1)}(I) = p^{(k)}(I)$
SET $\theta^{(k+1)}(I) = \theta^{(k)}(I)$
PROFYL 'P'
CALCULATE A(I), B(I), C(I)
D(I) $2 \leq I \leq M$
CALL TRADIA
STORE P(I)
$2 \leq I \leq M$
3
TEST CONVERGENCE
$P^{(k+1)}(I) - P^{(k)}(I)$
CALCULATE f(I)
CALL SIMPS
STORE f(I), $2 \leq I \leq M$
TEST CONVERGENCE
$f^{(k+1)}(I) - f^{(k)}(I)$
CALCULATE f(I)
CALL SIMPS
STORE f(I) $2 \leq I \leq M$
2
SET $\theta^{(k+1)}(I), \theta^{(k)}(I)$
6
PROFYL θ_l
CALCULATE A(I) B(I)
C(I), D(I) $2 \leq I \leq M$
CALL TRIDIA
STORE $\theta_l(I)$, $2 \leq I \leq M$
3
PROFYL y_o
CALCULATE $A_3(I)$, $B_3(I)$,
$C_3(I)$, $D_3(I)$, $2 \leq I \leq M$
CALL TRIDIA
STORE $y_o(I)$
$2 \leq I \leq M$
3
CALCULATE $y_{o,s}$
PROFYL y_f
CALCULATE AA(I), BB(I),
CC(I), DD(I) $2 \leq I \leq M$
CALL TRIDIA
STORE $y_f(I)$ $2 \leq I \leq M$
3
CALCULATE $y_{F,s}$
PROFYL 'θ'
CALCULATE $A_2(I)$, $B_2(I)$,
$C_2(I)$, $D_2(I)$ $2 \leq I \leq M$
CALL TRADIA
STORE $\theta(I)$ $2 \leq I \leq M$
3
TEST CONVERGENCE
$\theta^{(k+1)}(I) - \theta^{(k)}(I)$
CALCULATE θ_S & f_S
TEST CONVERGENCE
$f_S^{(k+1)} - f_S^{(k)}$
$\tau \rightarrow \tau + \Delta\tau$

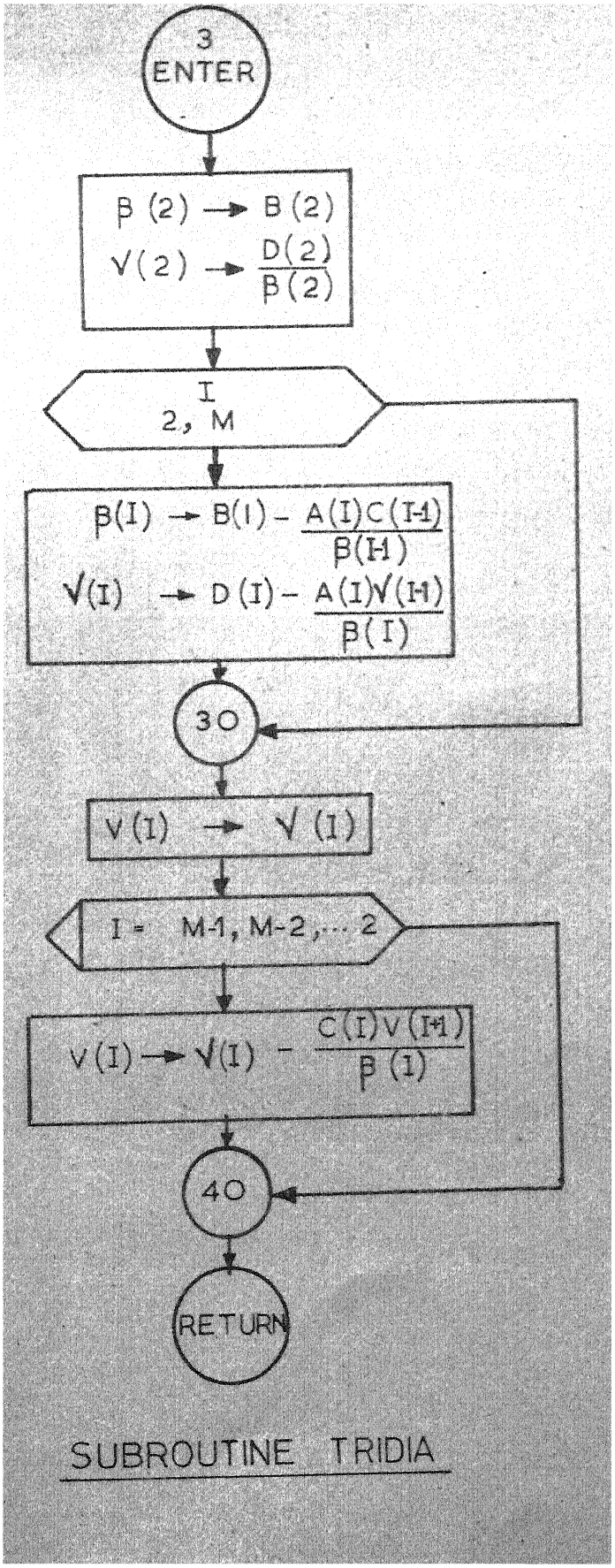

SUBROUTINE TRIDIA

A 42649

AE-1975-M-VEN-TRA